J. Fluid Mech. (1994), vol. 269, pp. 45–78

Circulation deposition on shock-accelerated planar and curved density-stratified interfaces: models and scaling laws

By RAVI SAMTANEY AND NORMAN J. ZABUSKY

Department of Mechanical and Aerospace Engineering, and CAIP Center, Rutgers University, Piscataway, NJ 08855, USA

(Received 12 May 1993 and in revised form 5 November 1993)

Vorticity is deposited baroclinically by shock waves on density inhomogeneities. In two dimensions, the circulation deposited on a *planar* interface may be derived analytically using shock polar analysis provided the shock refraction is *regular* . We present analytical expressions for Γ', the circulation deposited per unit length of the *unshocked* planar interface, within and beyond the regular refraction regime. To lowest order, Γ' scales as

$$\Gamma' \propto (1-\eta^{-\frac{1}{2}})(\sin\alpha)(1+M^{-1}+2M^{-2})(M-1)(\gamma^{\frac{1}{2}}/\gamma+1),$$

where M is the Mach number of the incident shock, η is the density ratio of the gases across the interface, α is the angle between the shock and the interface and γ is the ratio of specific heats for both gases. For $\alpha \leqslant 30°$, the error in this approximation is less than 10% for $1.0 < M \leqslant 1.32$ for all $\eta > 1$, and $5.8 \leqslant \eta \leqslant 32.6$ for all M. We validate our results by quantification of direct numerical simulations of the compressible Euler equations with a second-order Godunov code.

We generalize the results for total circulation on *non-planar* (sinusoidal and circular) interfaces. For the circular bubble case, we introduce a 'near-normality' ansatz and obtain a model for total circulation on the bubble surface that agrees well with results of direct numerical simulations. A comparison with other models in the literature is presented.

1. Introduction

The interactions of shock waves with density inhomogeneities are of fundamental importance in compressible turbulence, and occur in a myriad of situations, both in nature and in practical applications. This environment has been referred to as the shock-induced Rayleigh–Taylor instability or the *Richtmyer–Meshkov instability environment* after Richtmyer (1960) who did the linear stability analysis of long-wavelength perturbations on a vertical interface (figure 1*b*) subject to an impulsive acceleration, and Meshkov (1969) who provided the experimental confirmation. In recent years, there has been considerable interest in shock-induced mixing for scram-jet combustors (Yang, Kubota & Zukoski 1993), and inertial confinement fusion (Lindl, McCrory & Campbell 1992). Aspects of the light curve from supernova SN1987A may be explained by phenomena associated with the Richtmyer–Meshkov instability (Arnett *et al.* 1989).

Circulation deposition is the dominant fluid dynamical process in early-time

Richtmyer–Meshkov environments and it is imperative to quantify this process for model building and scaling. In this paper, we use shock polar analysis to obtain analytical expressions and scaling laws for circulation on density-stratified interfaces accelerated by planar shocks in *two-dimensional planar geometries*. We extend the analysis to predict the circulation on non-planar (sinusoidal and circular bubble) interfaces. Effects of changes in the ratio of specific heats across the interface are also examined.

The physical picture may be characterized by a shock wave propagating in a rectangular shock tube, through a gas of density ρ_0 and an interface separating a gas of density ρ_b. Figure 1 shows a schematic of three possible physical situations: a planar interface inclined at an angle, α; a sinusoidal interface with amplitude, A, and wavelength, λ ; or a bubble of radius normalized by the shock-tube width, r_0/L_T. The parameter space is three-dimensional: the strength of the shock characterized by the Mach number, M; the density ratio, $\eta = \rho_b/\rho_0$; and the geometry of the density interface characterized by α or A/λ or r_0/L_T. Two generic classes of interactions exist: one in which the shock crosses into a fluid with a higher sound speed, (the 'slow/fast' or s/f interaction), and a second where the shock passes into a region with a lower sound speed, ('fast/slow' or f/s). In this paper, we focus on f/s interactions where the interface is initially vorticity free. For simplicity, we have omitted the effects of viscosity and heat transfer, as they play a minor role in relevant physical experiments.

The vorticity equation for a two-dimensional inviscid flow is given by

$$\frac{\mathrm{D}(\omega/\rho)}{\mathrm{D}t} = (\nabla\rho \times \nabla p)/\rho^3. \tag{1.1}$$

As the shock strikes the density inhomogeneity it deposits a layer of vorticity due to baroclinic effects, i.e. a misalignment of density and pressure gradients. The physical phenomena may be classified into two distinct phases: the vorticity deposition phase which occurs when the incident shock is in contact with the interface; and the vorticity evolution phase coupled with secondary baroclinic effects which drive the flow after the primary incident shock leaves the interface. In this paper, we emphasize the vorticity deposition phase.

Early experimental work by Jahn (1956) examined the nature of shock wave refraction at gaseous interfaces. In this paper, we have made extensive use of shock polar analysis equations as presented by Henderson (1966). Abd-El-Fattah & Henderson (1978) described the transition of regular refraction to irregular refractions in terms of shock polar analysis at fast–slow interfaces. Henderson (1989) also discussed the refraction of shock waves in media with arbitrary equations of state and developed a rigorous definition of wave impedance which determines the nature of reflected and transmitted shocks, their intensities, and the fraction of energy and power that are reflected and transmitted. He showed that definitions of the interface in terms of density ratio and terms such as slow–fast or fast–slow may be misleading. Note that in this paper, the designation of interfaces in terms of density ratio was found to be adequate for the parameters chosen. A detailed account of shock wave refraction patterns at slow–fast interfaces, based on numerical studies, is given by Henderson, Colella & Puckett (1991). Further theoretical work on shock–contact interactions was done by Grove (1989).

Sturtevant (1985) experimentally investigated the s/f and f/s interaction of shocks with planar discontinuities, i.e. large-amplitude periodic sawtooth wave Richtmyer–Meshkov instability. The formation of a large stratified wall vortex was observed first in his experiments. The problem of shock-accelerated bubbles was addressed by

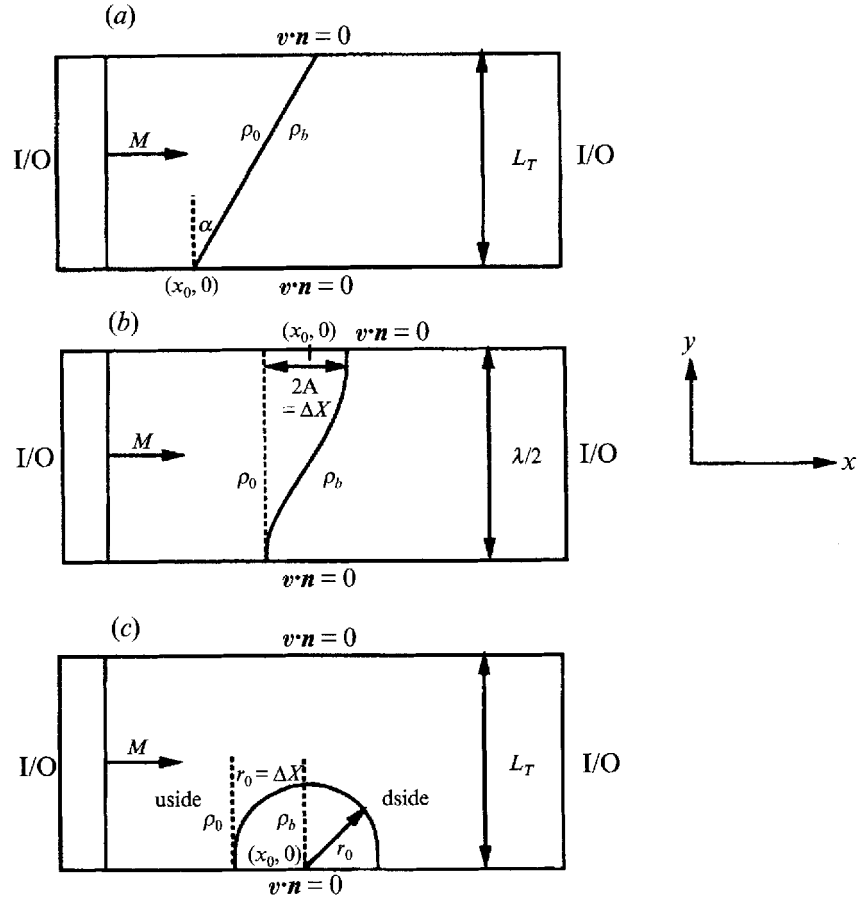

FIGURE 1. Schematic of physical domain and parameters for shock-accelerated density-stratified interfaces. (*a*) Planar interface; (*b*) sinusoidal interface; and (*c*) circular interface.

Rudinger & Sommers (1960) to investigate the motion of bubbles of different densities in accelerated gas flows. Haas & Sturtevant (1987) investigated experimentally the shock–cylinder, shock–sphere interactions for both the f/s and the s/f cases to examine the nature of shock refraction and diffraction. Winkler *et al.* (1987) did a parameter space survey of shock–sphere interactions using an axisymmetric PPM code and observed several interesting effects, notably the formation of a supersonic vortex in f/s interactions. A qualitative investigation of shock–planar interactions with vortex dominant effects at late time was presented by Hawley & Zabusky (1989). Picone & Boris (1988) presented results from direct numerical simulations (DNS) using the FCT scheme and developed an *ad hoc* model for the strength of the vortex in two-dimensional shock–bubble interactions.

The first quantitative investigation of vorticity generation in shock–planar interface interactions was presented by Yang *et al.* (1992). They obtained good comparison of their DNS results with the experimental shadowgraphs of Sturtevant (1985). Vorticity generation and late-time evolution and quantification of coherent vortical structures in shock–planar interface interactions ($M \leqslant 4.0$) were also investigated by Samtaney (1993) and Samtaney & Zabusky (1992*a*). They observed the roll-up of the initial

vortex layer into coherent vortices followed by late-time merger of some of these vortices, filamentation and formation of stratified dipolar vortices. The present work is an extension of the work on analytical quantification of circulation on shock accelerated f/s interfaces presented in Samtaney & Zabusky (1993). We also include some work on reduced models for circulation in shock–bubble interactions developed by Samtaney & Zabusky (1992*b*).

In §2 we present the equations of shock polar analysis and derive an exact expression and an asymptotic series for circulation on a planar f/s gas interface. In §3, we compare the circulation on the interface from numerical experiments with the analytical results. In §4, formulae with proper scaling behaviour are derived for the circulation on a planar interface. In §5, we derive the vorticity deposition by a shock on non-planar interfaces and present a model for the total circulation in two-dimensional shock–bubble interactions.

2. Circulation at a planar fast–slow gas interface

2.1. *Shock polar analysis equations*

A shock polar is the locus of final states that can be connected to a given initial state by a stationary oblique shock. For a planar interface the angle, α, between the incident shock and the interface is constant. Figure 2 shows a schematic of a shock at Mach number,M, refracting at a fast–slow planar interface (density ratio, η) inclined at an angle, α, to the vertical. The refraction is regular, i.e. all the shocks meet at a single node if α is smaller than a certain critical angle, α_{cr}. In shock polar analysis one assumes a frame of reference which is stationary with respect to the *node* where all the shocks meet. Furthermore, we assume that both gases are perfect and inviscid. In figure 2, *mm* is the interface; i, r, t are the incident, reflected and transmitted waves, respectively; $s1$ and $s2$ are the streamlines in the incident and transmitted media; δ_0 and δ_1 are the deflections of $s1$ due to i and r, respectively and δ_b is the deflection of $s2$ due to t. p_0 and p_b are the initial pressures in the incident and transmitted gases respectively†; p_1, p_2 and p_t are respectively the pressures behind the incident, reflected and transmitted waves. The free-stream Mach number in front (behind) the incident, reflected and transmitted shocks are $M_0(M_1)$, $M_1(M_2)$, and $M_b(M_t)$ respectively. γ_0 and γ_b are the ratios of specific heats in the incident and transmitted gases respectively.

Following Henderson (1966), we write equations of the shock polars as

$$\tan\delta_i(p) = -\frac{p/p_i - 1}{p/p_i - 1 - \gamma_i M_i^2}\left[\frac{(1+\mu_i^2)M_i^2 - \mu_i^2 - p/p_i}{\mu_i^2 + p/p_i}\right]^{\frac{1}{2}}, \tag{2.1}$$

where $i = 0, 1, b$ for the incident, reflected and transmitted shock, and $\mu_i^2 = (\gamma_i - 1)/(\gamma_i + 1)$ and $\gamma_0 = \gamma_1$. Note that in the shock polar plane (δ, p), where δ is the streamline deflection and p is the pressure ratio across the shock, the reflected polar is plotted with a shift from the origin of $(\delta_0(p_1), p_1)$. From the conservation laws we obtain

$$\frac{p_1}{p_0} = 1 + (1+\mu_0^2)(M^2 - 1), \tag{2.2}$$

† The gas in which the incident shock is initialized is loosely defined as the 'incident' gas. The gas on the other side of the interface is loosely defined as the 'transmitted' gas.

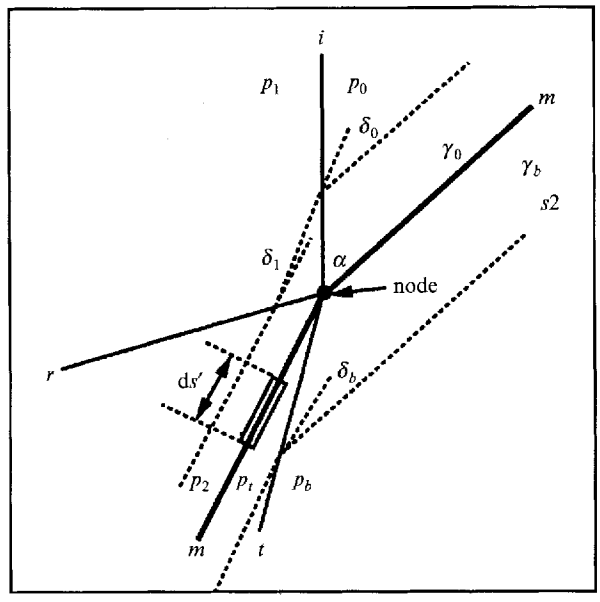

FIGURE 2. Schematic of regular refraction with three shocks at a fast–slow interface.

$$\frac{1+\frac{1}{2}(\gamma_0-1)M_0^2}{1+\frac{1}{2}(\gamma_0-1)M_1^2} = \psi(p_1/p_0, \mu_0), \tag{2.3}$$

where

$$\psi(\xi,\mu) \equiv \xi\frac{1+\mu^2\xi}{\mu^2+\xi}, \tag{2.4}$$

$$M_0 = M/\sin\alpha. \tag{2.5}$$

Since the velocity of the node is the same in both media, we have

$$M_b = M_0\eta^{\frac{1}{2}}\left(\gamma_0/\gamma_b\right)^{\frac{1}{2}}. \tag{2.6}$$

To solve for the pressure p_2, the following compatibility equations hold:

$$\delta_1(p_2) = \delta_0(p_1) - \delta_b(p_t), \tag{2.7}$$

$$\frac{p_t}{p_b} = \frac{p_2}{p_0} = \frac{p_2}{p_1}\frac{p_1}{p_0}. \tag{2.8}$$

Equation (2.8) may be written as a twelfth-order polynomial in p_2 (Henderson 1989). This polynomial may have more than one real root or no real roots. We concern ourselves with the *physical* root which is the smallest real root. We implicitly assume that no downstream pressure disturbances are imposed which will modify the solution.

If α is smaller than α_{cr} all the three waves are shocks and meet at a single node (called RRR). For very weak shock waves, as α is increased, the reflected wave becomes a Mach line and then a centred rarefaction fan (called RRE). As α is increased further the reflected wave is not a centred expansion fan and the refraction becomes anomalous. For stronger shocks the irregular refraction (called MRR) is typically characterized by the appearance of a Mach stem at the interface. For f/s interactions, transition from regular to irregular refractions occurs at three possible points: $min(M_1, M_2) = 1.0$, $M_t > 1$ and the mechanical equilibrium point. The latter

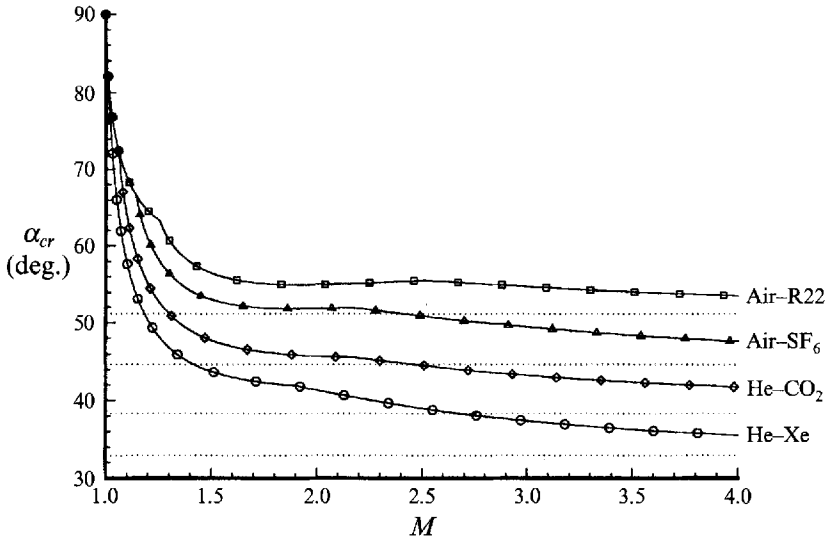

FIGURE 3. Critical angle, α_{cr}, for transition from regular to irregular refraction as a function of M. The dotted line is $\alpha_{cr} = \alpha_{cr\infty}$ for $M \to \infty$.

condition occurs when the intersection of the reflected and transmitted shock polars coincides with an intersection between the incident and transmitted shock polars. It is generally believed, based on experimental evidence, that the transition to irregularity occurs at the smallest angle, α, for which one of the above conditions holds. Note that for MRR cases where α_{cr} occurs at $M_2 = 1$, the slip line associated with the Mach stem is too weak to be observed. The domain of irregular refraction is quite complex and a detailed discussion of these cases is beyond the scope of this paper.

Using the above analytical criteria, we plot α_{cr} (figure 3) as a function of M for four physical interfaces: Air–R22 ($\eta = 3.0, \gamma_0 = 1.4, \gamma_b = 1.172$), Air–$SF_6$ ($\eta = 5.04, \gamma_0 = 1.4, \gamma_b = 1.0935$), He–$CO_2$ ($\eta = 11.0, \gamma_0 = 1.667, \gamma_b = 1.297$), and He–Xe ($\eta = 32.7, \gamma_0 = 1.667, \gamma_b = 1.667$). We observe that there is a certain critical Mach number beyond which the refraction proceeds from RRR to MRR instead of RRR to RRE. Below this Mach number, α_{cr} occurs at $M_1 = 1$ which is independent of η. Note that for smaller density ratios (as in the Air–R22, $\eta = 3$ case) α_{cr} is not necessarily monotonic with increase in M. This non-monotonic behaviour is even more severe for $\eta \approx 1$ (not shown).

2.2. *Normalizations*

For simplicity, we assume $p_b = p_0 = \rho_0 \equiv 1$ and $\rho_b = \eta$ initially . Thus, the sound speed is $\gamma_0^{\frac{1}{2}}$ in the incident gas. In the sections which follow we will normalize the circulation on the interface by a lengthscale which will be indicated. All the results will thus have units of circulation per unit length, i.e. units of velocity. In order to convert to physical units, our normalized circulation must be multiplied by the ratio of the physical sound speed to $\gamma_0^{\frac{1}{2}}$.

2.3. *Exact circulation*

Integrating the velocity along a contour of length ds′ parallel to the shocked interface and infinitely thin perpendicular to the interface (figure 2), we obtain the circulation

(vorticity deposition) per unit length of the *shocked* interface as

$$\frac{\mathrm{d}\Gamma}{\mathrm{d}s'} \equiv v_t - v_2, \tag{2.9}$$

where v_t and v_2 are the velocities tangential to the shocked interface in the transmitted gas and the twice-shocked incident gas, respectively. We renormalize the circulation with respect to the original *unshocked* interface by multiplying (2.9) by the geometric factor $\mathrm{d}s'/\mathrm{d}s = [\cos\alpha/\cos(\alpha - \delta_b)]$ which accounts for the instantaneous change in length of the interface due to the shock,

$$\Gamma' \equiv \frac{\mathrm{d}\Gamma}{\mathrm{d}s} = (v_t - v_2)\frac{\cos\alpha}{\cos(\alpha - \delta_b)}. \tag{2.10}$$

After some algebra (see the Appendix), the expression for Γ' reduces to

$$\Gamma' = \frac{\gamma_0^{\frac{1}{2}}}{\sin\alpha}\left(\left[M^2 + \frac{2}{\gamma_b - 1}\left(\frac{1 - \psi(p_2, \mu_b)}{\eta\gamma_0/\gamma_b}\right)\sin^2\alpha\right]^{\frac{1}{2}} - \left[M^2 + \frac{2}{\gamma_0 - 1}\left(1 - \psi(p_2/p_1, \mu_0)\psi(p_1, \mu_0)\right)\sin^2\alpha\right]^{\frac{1}{2}}\right)\frac{\cos\alpha}{\cos(\alpha - \delta_b)}. \tag{2.11}$$

Note that $\sin\alpha$ in (2.11) has the same sign as $\nabla\rho \times \nabla p$.

In the above equation, $\psi^{\frac{1}{2}}$ represents physically the ratio of sound speed behind and ahead of a shock. Equation (2.11) may only be used for RRR at a planar interface and we refer to it as the 'exact' shock polar result for Γ'. Typically, for a slow–fast interface the shock refraction is of the RRE type for small α (Henderson *et al.* 1991). For RRE one may derive a corresponding equation for circulation by replacing the shock jump conditions across the reflected wave with the Prandtl–Meyer expansion conditions.

2.4. *Approximate circulation at a fast–slow gas interface*

Upon transition to irregularity the shock polar equations do not yield any *physical* root. We expand Γ' in (2.11) as a series in $\sin\alpha$ about $\sin\alpha = 0$. By symmetry arguments, the circulation on the interface is an odd function of $\sin\alpha$. The pressure, p_2, behind the transmitted or reflected shock is at most second order in $\sin\alpha$. Thus

$$\Gamma' = \Gamma_1'\sin\alpha + \Gamma_3'\sin^3\alpha + O(\sin^5\alpha), \tag{2.12}$$

where

$$\Gamma_1' = \left.\frac{\partial\Gamma'}{\partial\sin\alpha}\right|_{\sin\alpha=0}. \tag{2.13}$$

This reduces to

$$\Gamma_1' = \frac{\gamma_0^{\frac{1}{2}}}{M}\left(\frac{1}{\gamma_b - 1}\frac{1 - \psi(p_{20}, \mu_b)}{\eta\gamma_0/\gamma_b} - \frac{1}{\gamma_0 - 1}\left(1 - \psi(p_{20}/p_1, \mu_0)\psi(p_1, \mu_0)\right)\right), \tag{2.14}$$

where the limiting pressure $p_{20} = \lim_{\alpha\to 0} p_2$ behind the reflected shock is governed by the following nonlinear algebraic equation:

$$\frac{p_1 - 1}{(\mu_0^2 + p_1)^{\frac{1}{2}}} - \frac{p_{20}/p_1 - 1}{(\mu_0^2 + p_{20}/p_1)^{\frac{1}{2}}}\psi^{\frac{1}{2}}(p_1, \mu_0) - \eta^{-\frac{1}{2}}\frac{p_{20} - 1}{(\mu_b^2 + p_{20})^{\frac{1}{2}}}\left(\frac{\gamma_0 + 1}{\gamma_b + 1}\right)^{\frac{1}{2}} = 0. \tag{2.15}$$

The derivation of Γ_3' is given in the Appendix. The series expansion (2.12) is truncated after one or two terms and is referred to as the 'approximate' shock polar result for circulation. Thus the approximate result to first order is given by

$$\tilde{\Gamma}_1' = \Gamma_1' \sin\alpha, \tag{2.16}$$

and to third order is given by

$$\tilde{\Gamma}_3' = \Gamma_1' \sin\alpha + \Gamma_3' \sin^3\alpha. \tag{2.17}$$

Unlike the exact result, Γ_1' and Γ_3' are real for $0 \leqslant \alpha \leqslant \pi/2$. As shown later, the third-order term contributes only negligibly to the total circulation. Furthermore, we believe that higher-order terms do not contribute significantly to the circulation.

2.5. *Effects of changes in ratio of specific heats*

So far we have assumed that the ratio of specific heats is different for each gas. In the past, some studies (Yang *et al.* 1992; Zabusky *et al.* 1992) have assumed the same ratio of specific heat in both gases. Although for large M this may not be a good assumption, we note that differences in γ across the interface lead to a small change in the Γ'. Let Γ_{11}' be the circulation per unit original length of the interface if the correct specific heat ratios are used for the gases. Let Γ_{12}' be the circulation per unit original length of the interface which is evaluated by changing γ_b. For the interfaces considered above we plot $[\Gamma] = \Gamma_{11}' - \Gamma_{12}'$ normalized by Γ_{11}' for $\alpha = 45°$ interfaces. Note that for an He–Xe interface, for $\alpha = 45°$ there is no shock polar solution for $M > 1.4$ and so we have only plotted the $M = 1.05$ and $M = 1.2$ cases in figure 4. We observe in figure 4 that the changes in the ratio of specific heat across the interface does not significantly affect the initial vorticity deposition. Using this fact we will assume that $\gamma_b = \gamma_0$ for simplicity in deriving scaling laws in §4.

2.6. *Convective Mach number*

We define an average convective Mach number, as done for shear layers, as

$$M_c = \frac{|v_2 - v_t|}{c_2 + c_t} = \frac{|\Gamma'|}{c_2 + c_t}. \tag{2.18}$$

The velocity difference $v_2 - v_t$ is the same as the circulation per unit length Γ' and c_2, c_t are the sound speeds in the incident and transmitted gases after shock refraction. The convective Mach number, M_c, is a measure of compressibility. As given in (2.18), M_c can be calculated only for RRR. Note that the leading term in the series expansion of c_2 and c_t (which are even functions of $\sin\alpha$) in $\sin\alpha$ is of $O(\sin^2\alpha)$. Therefore, to first order M_c may be written as

$$M_c = \frac{|\tilde{\Gamma}_1'|}{c_{20} + c_{t0}} + O(\sin^3\alpha), \tag{2.19}$$

where $c_{20} = \lim_{\alpha\to 0} c_2$ and $c_{t0} = \lim_{\alpha\to 0} c_t$ are obtained from a one-dimensional interaction.

In figure 5, M_c is plotted as a function of M for four interfaces. The angle α is chosen as 90° so that for an interface inclined at smaller angles, M_c has to be multiplied by $\sin\alpha$. Note that for large M the change in M_c is very small as M increases. For most cases, M_c is small enough for the flow to be considered incompressible after the shock passage.

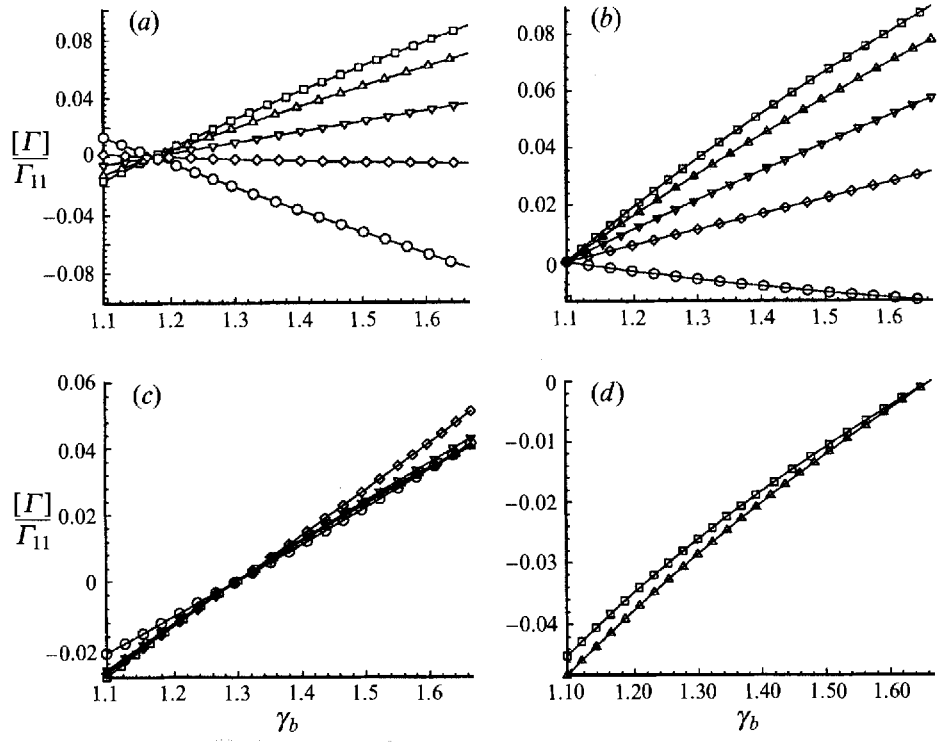

FIGURE 4. Difference in circulation $[\Gamma] = \Gamma_{12} - \Gamma_{11}$ normalized by Γ_{11} where Γ_{11} is the circulation when true γ_0, γ_b are used and Γ_{12} is the circulation obtained by changing γ_b. The angle of the interface is $\alpha = 45°$. The Mach numbers of the incident shock are: $M = 1.05(\square), 1.2(\triangle), 1.5(\triangledown), 2.0(\diamond), 4.0(\bigcirc)$. The interfaces are: (*a*) Air–R22; (*b*) Air–SF_6; (*c*) He–CO_2; and (*d*) He–Xe.

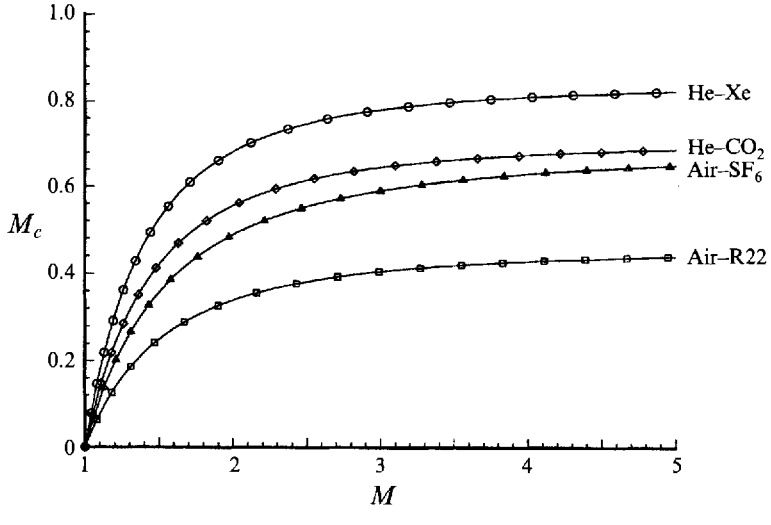

FIGURE 5. Convective Mach number, M_c, *vs.* incident shock Mach number, M, for four interfaces.

3. DNS and quantification

3.1. *Governing equations and physical parameters*

In this section, we compare the exact and approximate circulation ($\Gamma', \tilde{\Gamma}_1', \tilde{\Gamma}_3'$) with the circulation ($\hat{\Gamma}'$) obtained from direct numerical simulations (DNS) of two-dimensional compressible Euler equations on a uniform grid with $\Delta x = \Delta y = 1.0$. The governing equations in conservative form are

$$\boldsymbol{U}_t + \mathscr{F}(\boldsymbol{U})_x + \mathscr{G}(\boldsymbol{U})_y = 0, \tag{3.1}$$

where $\boldsymbol{U} = \{\rho, u, v, E, \rho\zeta\}^T$, $\mathscr{F}(\boldsymbol{U}) = \{\rho u, \rho u^2 + p, \rho uv, (E+p)u, \rho\zeta u\}^T$ and $\mathscr{G}(\boldsymbol{U}) = \{\rho v, \rho uv, \rho v^2 + p, (E+p)v, \rho\zeta v\}^T$. E is the total energy related to the pressure, p, by $p = (\gamma - 1)(E - \frac{1}{2}\rho(u^2+v^2))$; and ζ is the interface tracking function. We have used the conservative level-set formulation (Mulder, Osher & Sethian 1992) in which a function $\zeta(\boldsymbol{x}, t)$ is defined everywhere in the domain. Then a particular value of $\zeta(\boldsymbol{x}, t)$ defines the interface. In our case we initialize $\zeta(\boldsymbol{x}, 0) = +1(-1)$ in the incident (transmitted) gas. Thus, the level set $\zeta(\boldsymbol{x}, t) = 0$ defines the interface at all times. The last PDE in the system of equations (3.1) governs $\zeta(\boldsymbol{x}, t)$ and is coupled to the other equations through the variable $\gamma(\boldsymbol{x}, t)$. We observe that expressing the level-set function in conservative form leads to an additional equation in the system of conservation laws and this system is *not strictly* hyperbolic.

The boundary conditions are reflecting in the y-direction and inflow/outflow in the x-direction. We use four physical interfaces which correspond to a large span of density ratios: Air–R22 ($\eta = 3.0, \gamma_0 = 1.4, \gamma_b = 1.172$), Air–$SF_6$ ($\eta = 5.04, \gamma_0 = 1.4, \gamma_b = 1.0935$), He–$CO_2$ ($\eta = 11.0, \gamma_0 = 1.667, \gamma_b = 1.297$), and He–Xe ($\eta = 32.7, \gamma_0 = 1.667, \gamma_b = 1.667$). The interfaces were planar and inclined at different angles to the vertical ($\alpha = 15°, 30°, 45°, 60°, 75°$). The incident shock strengths were: $M = 1.05, 1.5, 4.0$.

For each of these runs we initialized the interface at about $x = 120\Delta x$ and initialized the shock by about $X_0 \approx 10\Delta x$ to the left of the density interface which is spread over $2\Delta x$ to $3\Delta x$. The width of the shock tube was fixed at $L_T = 80\Delta y$ in all simulations described in this section. The domain size in the x-direction was increased as the angle, α between the shock and the interface increased.

3.2. *Numerical method*

Our numerical method, a generalization of Godunov's method, is second-order accurate in space and time and includes interface tracking. The method is based on Chern's method (I.-L. Chern, private communication 1991) and is similar to the Eulerian MUSCL (Colella 1985) scheme which is suitable for flows involving nonlinear wave interactions. We make the following assumptions: the flow is inviscid, the gases are perfect and there is no chemical reaction between the gases which are further assumed to be in thermal equilibrium.

The solution at each time step is interpolated to give a 'piecewise linear' distribution in each grid zone. Van Leer's monotonicity constraints (Van Leer 1977) are used to mitigate short-wavelength numerical oscillations. The linearized characteristic equations are solved to get the solution at an intermediate time step. The flux terms are then obtained at each cell boundary by solving the full nonlinear one-dimensional Riemann problem (Smoller 1982). In our implementation, we use $\zeta(\boldsymbol{x}, t)$ to determine the volume fraction of the gases in each cell where $|\zeta(\boldsymbol{x}, t)| < 1$. We use alternating sweeps in the x- and y-directions, which formally yields second-order accuracy (Strang 1968).

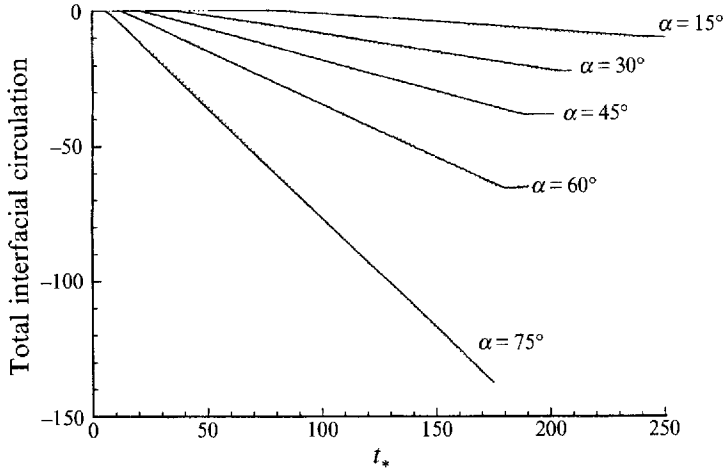

FIGURE 6. Convergence test for total circulation on the interface, $\hat{\Gamma}$, as a function of time, $t_* = t\tan(\alpha)/\tan(75°)$. Solid line is for $(L_T, \Delta y) = (160\Delta y, 0.5)$ and the dotted line is for $(L_T, \Delta y) = (80\Delta y, 1.0)$. The incident shock Mach number is $M = 1.5$. Air–R22 interface.

The details of the numerical method are given in Samtaney (1993). Good agreement with the shock-tube experiments of Sturtevant (1985) was observed by Samtaney (1993) using different ratios of specific heats and tracking the interface by the level-set method. Note that this numerical method is the same as used by Yang *et al.* (1992) though they did not track the interface and assumed the same ratio of specific heats for both gases. A convergence study of the numerical method was presented by Yang *et al.* (1992). Convergence tests for the numerical method with interface tracking are presented in Samtaney (1993). Therefore, only a brief convergence study is presented below.

3.3. *Visiometrics and results*

We now quantify the circulation using DNS and show convergence to the exact circulation result where it exists and to the approximate formulae. At any instant the total vorticity on the interface is calculated as,

$$\hat{\Gamma}(t) = \sum_D \omega(i,j,t)\Delta x \Delta y, \tag{3.2}$$

where $D = \{(i,j,t) \quad \text{such that} \quad |\zeta(i,j,t) < 1|\}$, and

$$\omega(i,j,t) = \frac{v(i+1,j,t) - v(i-1,j,t)}{2\Delta x} - \frac{u(i,j+1,t) - u(i,j-1,t)}{2\Delta y}. \tag{3.3}$$

In a convergence study, we use two cases, $(L_T, \Delta y) = (80\Delta y, 1.0)$, and $(L_T, \Delta y) = (160\Delta y, 0.5)$. For these two resolutions, we plot the total interfacial circulation, $\hat{\Gamma}$, as a function of time, $t_* = t\tan(\alpha)/\tan(75°)$ for $M = 1.5$ shock interaction at an Air-R22 interface inclined at $\alpha = 15°, 30°, 45°, 60°, 75°$ (see figure 6). We observe very good agreement for total interfacial circulation at the two resolutions. All the other results presented in this section use $(L_T, \Delta y) = (80\Delta y, 1.0)$.

We ran the code until the shock traversed the complete interface, i.e. until $t_s = (L_T \tan\alpha + X_0)/V_s$ where V_s is the speed of the incident shock. We then calculated the total interfacial circulation on the interface at this time. We divide $\hat{\Gamma}$ by

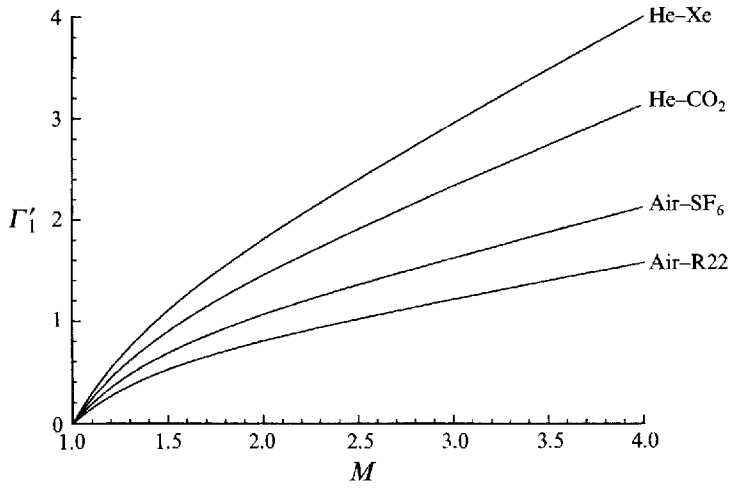

FIGURE 7. Leading-term coefficient, Γ_1', in the $\sin\alpha$ series expansion of Γ' as a function of M for four interfaces.

$l(= L_T/\cos\alpha)$ to get the numerical value of the circulation per unit length of the original interface ($\hat{\Gamma}'$). In figures 8, 9, and 10 we show Γ', the exact result (2.11); $\tilde{\Gamma}_3'$, the approximate circulation; and $\hat{\Gamma}'$, the numerical result normalized by $\tilde{\Gamma}_1'$. To facilitate the calculation of all the quantities, Γ_1' is plotted as a function of M for the four interfaces (figure 7). In figures 8, 9, and 10 the exact result (2.11) terminates at α_{cr} while the approximate results can be extended to $\alpha = \pi/2$. For most cases, Γ', $\tilde{\Gamma}_1'$, and $\tilde{\Gamma}_3'$ agree very well with each other and with the numerical result ($\hat{\Gamma}'$) up to moderate values of α. Also the agreement is better for larger Mach numbers and smaller density ratios. For weak shocks, $\tilde{\Gamma}_1'$ differs considerably from Γ'. However, the third-order correction makes the agreement quite good.

We now discuss the discrepancies between the numerical result ($\hat{\Gamma}'$) and the anayt-ical results (Γ', $\tilde{\Gamma}_1'$ and $\tilde{\Gamma}_3'$) at large α and large η. These discrepancies arise from the: (i) comparison of time varying processes (both physical and numerical) with a stationary result; (ii) regular and irregular reflection of the transmitted shock at the lower boundary; (iii) proximity of the shock to the diagnosed contact surface domain; (iv) comparison of the process of irregular refraction at the interface with an asymptotic series. For example, in figure 11 we show greyscale images, using DAVID (Bitz & Zabusky, 1990), of $\sinh^{-1}(\omega)$ for an Air–SF_6 interface shocked by $M = 1.05(a), 1.5(b), 4.0(c)$ shocks at $t_s \approx (L_T \tan\alpha + X_0)/V_s$. The images from left to right are for $\alpha = 15°, 30°, 45°, 60°, 75°$. (The arcsinh transformation enhances low-amplitude vorticity seen clearly on the reflected and transmitted shocks.) For large α the vortex layer rolls up near the lower wall to form a coherent vortex which has weak baroclinicity associated with it. The lower wall vortex binds with its image and translates in the upstream direction. For $M = 1.05$ the vortex layer is straight for $\alpha < 60°$. At $\alpha = 60°, 75°$ the transmitted shock reflects off the lower boundary and interacts with the vortex layer. For $\alpha = 75°$ the refraction is irregular and secondary multiple refractions occur near the lower boundary; the vortex layer is no longer straight. For $M = 1.5$, there is a Mach stem where the transmitted shock meets the lower boundary due to the interaction of the transmitted shock and associated opposite-signed vorticity layer (shown in black). With respect to item (iv) above,

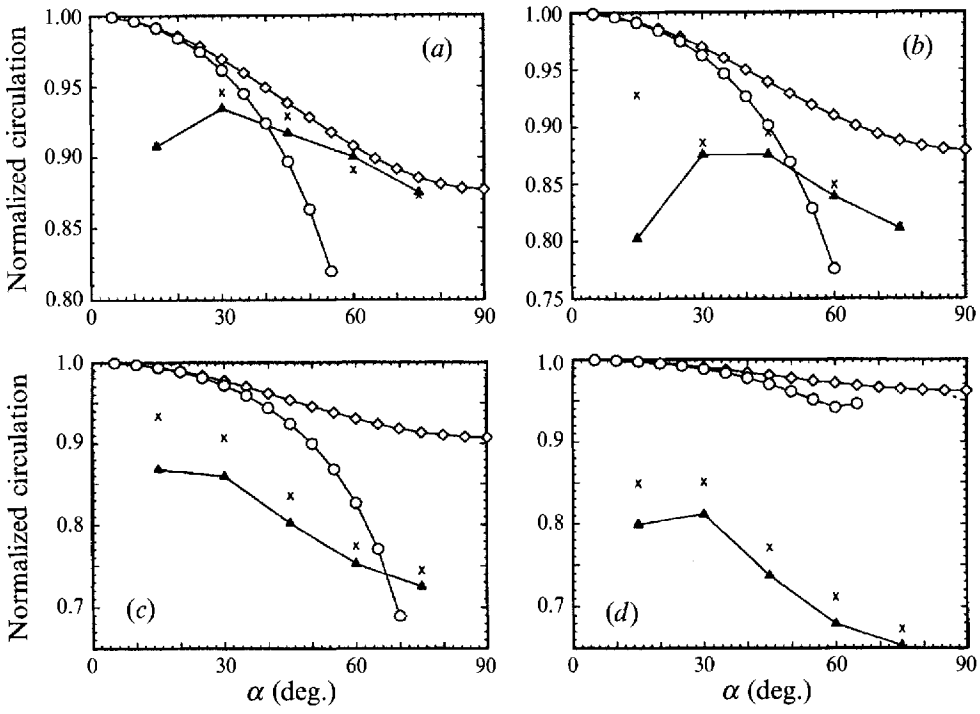

FIGURE 8. Circulation per unit *original* length, Γ' for Mach 1.05 shock interactions with (*a*) Air–R22 interface; (*b*) Air–SF_6 interface; (*c*) He–CO_2 interface; (*d*) He–Xe interface. ○, $\Gamma''/\tilde{\Gamma}_1'$ (circulation per unit original length of the interface normalized by the first-order term, $\tilde{\Gamma}_1'$); ◇, $\tilde{\Gamma}_3'/\tilde{\Gamma}_1'$ (circulation up to third order in $\sin\alpha$ series normalized by $\tilde{\Gamma}_1'$); ▲, ×, $= \hat{\Gamma}'/\tilde{\Gamma}_1'$ (circulation in DNS normalized by $\tilde{\Gamma}_1'$).

although the refraction is MRR at $\alpha = 60°$ the Mach stem near the contact surface associated with this irregularity is poorly resolved and the slip line is too weak to be observed. The refraction at $\alpha = 75°$ is also irregular and the lower part of the vortex layer has evolved substantially; secondary baroclinic processes occur close to the lower boundary and we observe the generation of opposite-signed vorticity. Similar and stronger processes occur for $M = 4.0$. The transmitted shock is very close to the interface and the opposite-signed vorticity is also very close to the interface. This affects the numerical quantification process. We also recognize that implicit numerical viscosity increases the width of the vortex layer and affects all these processes.

To overcome the difficulty of the time-varying processes, we also use a temporal sampling technique to quantify $\hat{\Gamma}'$ as

$$\hat{\Gamma}' = \frac{1}{N}\sum_{i}^{N} \frac{\hat{\Gamma}(t_i + \Delta t) - \hat{\Gamma}(t_i - \Delta t)}{2\Delta l}, \tag{3.4}$$

where $\Delta l = \Delta t(V_s/\sin\alpha)$ and $\hat{\Gamma}(t_i)$ is the total interfacial circulation in the domain at time t_i. We calculate the average of N samples (for an Air–R22 interface, $M = 1.5$, and $\alpha = 15°, 30°, 45°, 60°, 75°$, $N = 10, 30, 60, 100$ and 200 respectively). The results of this quantification are labelled × in figures 8, 9, and 10 and one observes a decrease in the discrepancy, especially for large-η cases.

Although the circulation per unit length of the shocked interface, $\mathrm{d}\Gamma/\mathrm{d}s'$ (2.9), is

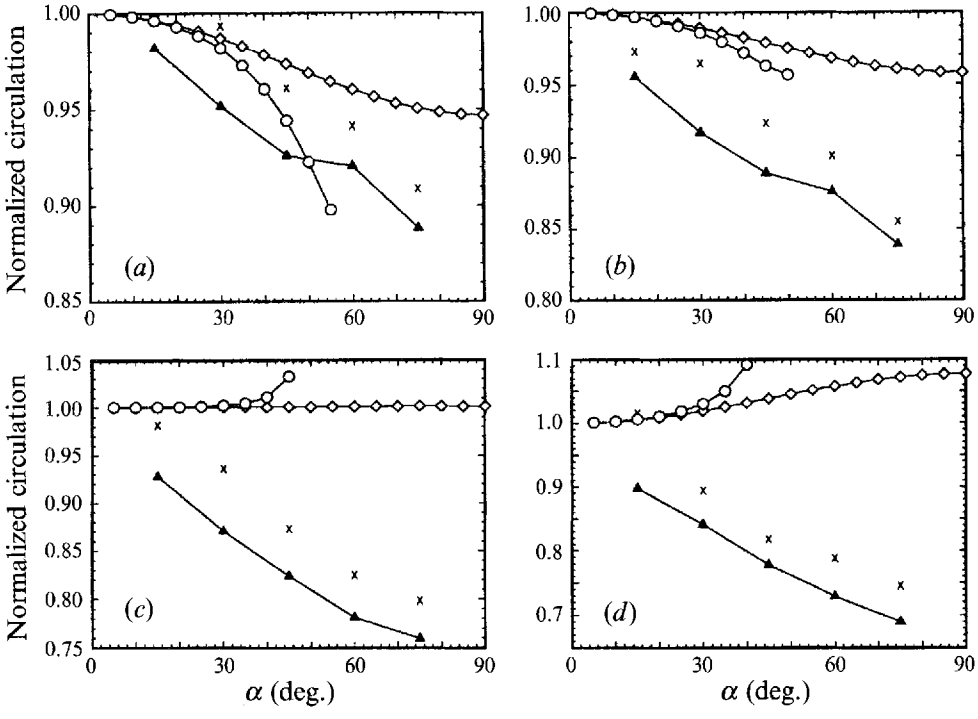

FIGURE 9. As figure 8 but for a Mach 1.5 shock.

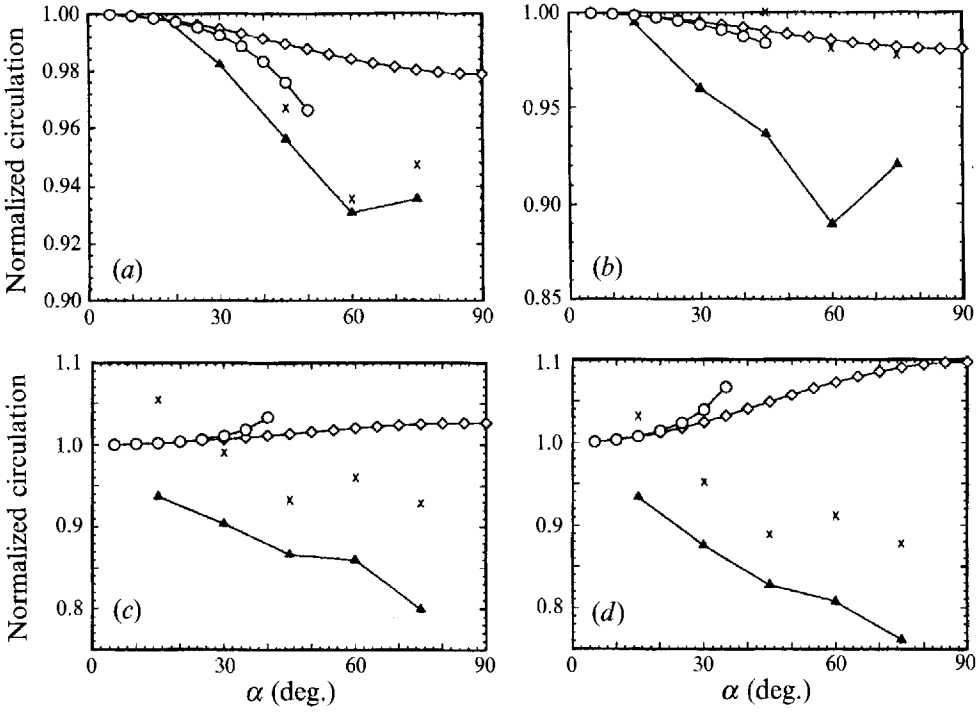

FIGURE 10. As figure 9 but for a Mach 4.0 shock.

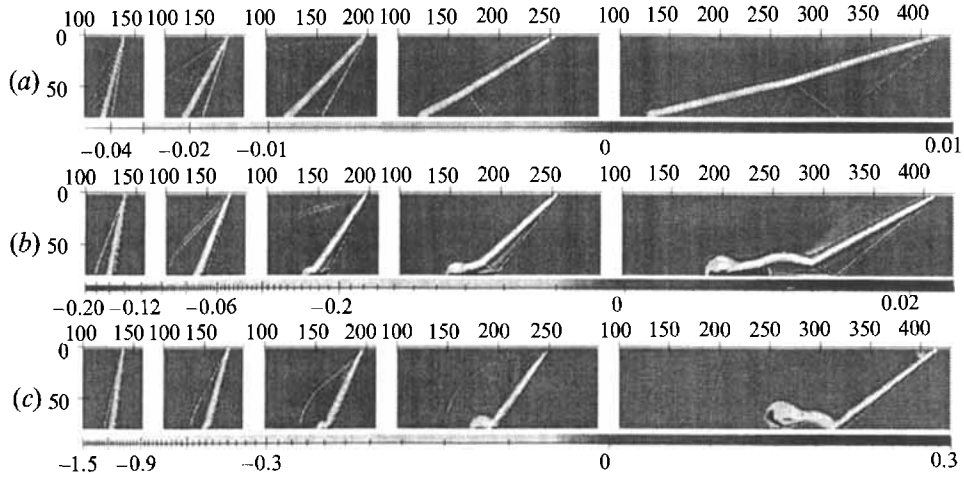

FIGURE 11. Vorticity images for an Air–SF_6 interface. (*a*) $M = 10.5$; (*b*) $M = 1.5$, (*c*) $M = 4.0$. Left to right: $\alpha = 15°, 30°, 45°, 60°, 75°$

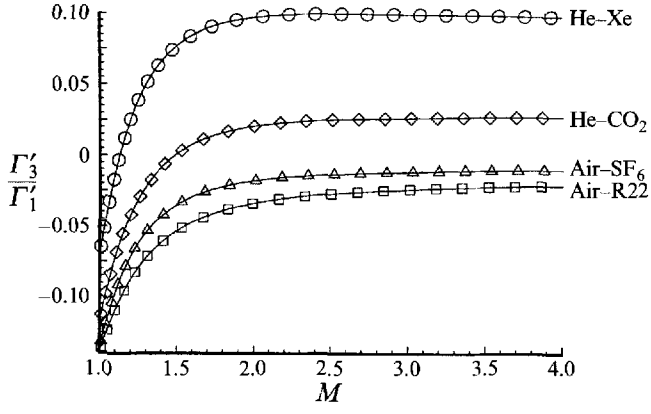

FIGURE 12. Ratio of third-order term, Γ_3', to the first-order term, Γ_1', in the series expansion of Γ' in $\sin\alpha$, as a function of M.

a monotonic function of α, the corrected circulation, Γ' (2.10), is not monotonic for weak shocks. The reason is that $\cos\alpha$ in the length correction term becomes small for large α, especially near the transition from RRR to RRE.

In figure 12 we plot the ratio of Γ_3' to Γ_1' for various cases. In most cases the ratio is a very small number. The third-order term contributes more significantly for small Mach numbers where the refraction is approaching RRE.

To verify that the approximate expression is valid for large angles we need interfaces where we encounter large angles but where the time of passage of the shock is small. This we defer until the section on non-planar interfaces.

4. Scaling laws

Although we have the exact expression for circulation on a planar fast–slow gas interface, this expression is coupled with the equations of shock polar analysis

through the evaluation of the pressure behind the reflected and transmitted shocks. It is desirable to derive certain scaling laws which may prove useful in a certain region of our three-dimensional parameter domain. In this section we present scaling laws for Γ' in terms of M, η, α and γ. We assume for simplicity that $\gamma_0 = \gamma_b$, for which $\eta^{\frac{1}{2}}$ is the ratio of sound speed across the interface. The scaling laws are based on the asymptotic series of Γ' in the regular refraction regime. We examine the behaviour of the leading term in the asymptotic series and if the leading term approximates the exact circulation with a 'small error', we use the expansion variable as a scaling factor.

It was demonstrated in §2 that the leading term in the series expansion of Γ' in $\sin\alpha$ approximates Γ' accurately for several cases. Thus an appropriate *scaling factor for the inclination of the interface is* $\sin\alpha$.

4.1. *Circulation for very strong incident shocks*

Consider the case of an infinitely strong shock $M \to \infty$. The subscript ∞ is used to indicate the limit as $M \to \infty$. The equations of shock polars reduce to

$$\tan\delta_{0\infty} = \frac{\sin 2\alpha}{\gamma + 1 - 2\sin^2\alpha}, \tag{4.1}$$

$$\tan\delta_{b\infty}(p_\infty) = \frac{p_\infty^{\frac{1}{2}}\sin\alpha}{\gamma\eta - p_\infty\sin^2\alpha}\left[(1+\mu^2)\eta - p_\infty\sin^2\alpha\right]^{\frac{1}{2}}, \tag{4.2}$$

$$\tan\delta_{1\infty}(p_\infty) = \frac{p_\infty - (1+\mu^2)}{(1+\gamma M_1^2)(1+\mu^2) - p_\infty}\left[\frac{((1+\mu^2)M_1^2 - \mu^2)(1+\mu^2) - p_\infty}{\mu^2(1+\mu^2) + p_\infty}\right]^{\frac{1}{2}}, \tag{4.3}$$

$$M_1^2 = \frac{2}{\gamma - 1}\left[\frac{(\gamma+1)^2}{4\gamma}\frac{1}{\sin^2\alpha} - 1\right], \tag{4.4}$$

$$\delta_{1\infty}(p_\infty) = \delta_{0\infty} - \delta_{b\infty}(p_\infty). \tag{4.5}$$

The above equations may be solved for $p_\infty = p_2/M^2$. For $M \to \infty$, we observe that p_∞ and $\delta_{b\infty}$ approach asymptotic values. Γ'/M also asymptotes to a lower bound given by

$$\frac{\Gamma'}{M} \to \frac{\gamma^{\frac{1}{2}}}{\sin\alpha}\left[\left(1 - \frac{2}{\gamma+1}\frac{p_\infty}{\eta}\sin^2\alpha\right)^{\frac{1}{2}} - \left(1 - \frac{2}{\gamma+1}\frac{1+\mu^2+p_\infty}{1/\mu^2 + (1+\mu^2)/p_\infty}\sin^2\alpha\right)^{\frac{1}{2}}\right]\frac{\cos\alpha}{\cos(\alpha - \delta_{b\infty})}. \tag{4.6}$$

The above result implies that *for very strong incident shocks, Γ' scales linearly in M*.

Another important observation is that $\alpha_{cr} = \alpha_{cr\infty}$ has a finite lower bound. We have assumed implicitly that the transition criterion from RRR to MRR does not change for $M \to \infty$. In figure 3 $\alpha_{cr\infty}$ is plotted as the dotted line for four interfaces.

The turning angle, δ_b, which is a measure of the instantaneous compression of the interface by the shock, has an upper bound given by $\delta_{b\infty}$. For instance, an Air–R22 interface inclined at $\alpha = 45°$ has $\delta_{b\infty} = 27.2°$. This is a restatement of the fact from normal shock theory that an infinitely strong shock has an upper limit on the compression it causes as it moves through a gas.

4.2. *Circulation for weak shocks*

We now express Γ' as a series expansion for weak shocks ($M \to 1$). The expansion variable is a function of Mach number such that it asymptotes to M for large M and leads to zero circulation for $M = 1$. Thus let $\xi(M)$ be the expansion variable. Γ' is expressed as

$$\Gamma' = \left.\frac{\partial \Gamma'}{\partial \xi}\right|_{\xi=0} \xi + \left.\frac{\partial \Gamma'}{\partial p_2}\right|_{\xi=0} (p_2 - 1) + O(\xi^2). \tag{4.7}$$

One then expresses p_2 as a series in ξ using the shock polars. One has mathematical freedom in choosing the expansion variable, $\xi(M)$. We investigated several $\xi(M)$ having the form

$$\xi(M) = \frac{P(M)}{Q(M)}, \tag{4.8}$$

where $P(M), Q(M)$ are polynomials of degree n and $n-1$ respectively. This gives a linear behaviour in M for large M which was established in an earlier section. The form finally chosen gives the 'smallest error' in the parameter space explored and is given by

$$\xi(M) = (1 + M^{-1} + 2M^{-2})(M - 1). \tag{4.9}$$

After some algebra, we get

$$\Gamma' = \left[\frac{\gamma^{\frac{1}{2}}}{\gamma+1}\frac{\eta-1}{\eta^{\frac{1}{2}}}\frac{\sin 2\alpha}{\cos\alpha' + \eta^{\frac{1}{2}}\cos\alpha}\right](1 + M^{-1} + 2M^{-2})(M-1) + O(\xi^2), \tag{4.10}$$

where $\sin\alpha' = \sin\alpha/\eta^{\frac{1}{2}}$. Note that this result is not monotonic in α. There is a certain maximum which occurs at α_*, a root of the polynomial

$$(\eta+1)\cos^8\alpha + (\eta^2-4)\cos^6\alpha + (-4\eta+6)\cos^4\alpha + 4(\eta-1)\cos^2\alpha - \eta + 1 = 0. \tag{4.11}$$

Note that α_* is not related to the transition to irregularity. In figure 13 we plot Γ', (2.11), the leading term in (4.10), and results from DNS quantification ($\hat{\Gamma}'$), as a function of M for three planar interfaces ($\eta = 3.0, 5.04, 11.0$) inclined at $\alpha = 45°$. We observe that the leading term in the above series expansion approximates the exact result for a large range in M. The agreement is even better for smaller angles, which are not plotted. The dotted line in these plots shows the asymptotic value as indicated by the $M \to \infty$ result. Expressing the circulation as a series for weak shocks and small inclinations of the interface, we get

$$\Gamma' = \frac{2\gamma^{\frac{1}{2}}}{\gamma+1}\frac{\eta^{\frac{1}{2}}-1}{\eta^{\frac{1}{2}}}\sin\alpha(1 + M^{-1} + 2M^{-2})(M-1) + O(\xi^2) + O(\sin^3\alpha). \tag{4.12}$$

4.3. *Circulation for small density ratios*

In this section we examine the behaviour of small density jumps across the interface. We express the circulation as a series in $\eta' = 1 - \eta^{-\frac{1}{2}}$. The expansion variable was chosen by examining the behaviour of circulation for weak shocks and small inclinations, (4.12). Thus the circulation is given by

$$\Gamma' = \left.\frac{\partial \Gamma'}{\partial \eta'}\right|_{\eta'=0} \eta' + \left.\frac{\partial \Gamma'}{\partial p_2}\right|_{\eta'=0} (p_2 - p_1) + O(\eta'^2). \tag{4.13}$$

Note that in the limiting case of a zero density gradient across the interface the

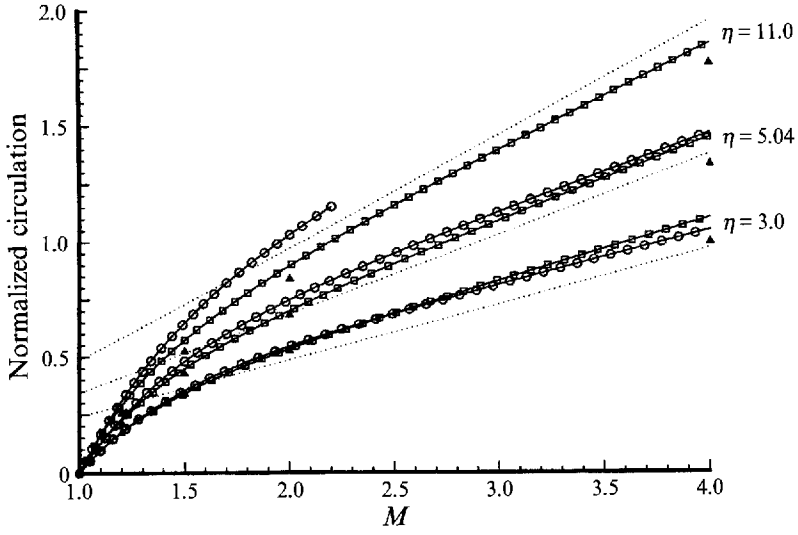

FIGURE 13. Circulation per unit *original* length as a function of M. The angle of the interface is $\alpha = 45°$. The density ratio is indicated in the figure. ○, Γ'; □, leading term in series of Γ' in $\xi(M) = (1 + M^{-1} + 2M^{-2})(M - 1)$; ▲, $\hat{\Gamma}'$. The dotted line is the asymptotic limit of Γ' for $M \to \infty$.

pressure behind the reflected wave is the same as the pressure behind the original incident shock. We express the pressure behind the reflected shock using the shock polar equations:

$$p_2 = p_1 + \left[\frac{-\partial\delta_b/\partial\eta'}{\partial\delta_b/\partial p_2 + \partial\delta_1/\partial p_2}\right]_{\eta'=0} \eta', \tag{4.14}$$

$$\left.\frac{\partial\delta_b}{\partial\eta'}\right|_{\eta'=0} = -\sin 2\delta_0 \left[\frac{(\gamma+1)M^2}{(\gamma+1)M^2 - 2(M^2-1)\sin^2\alpha} - \frac{1}{2\cos^2\alpha}\right], \tag{4.15}$$

$$\left.\frac{\partial\delta_b}{\partial p_2}\right|_{\eta'=0} = \frac{(\gamma+1)\sin 2\delta_0}{4\gamma} \left[\frac{(\gamma+1)M^2/(M^2-1)}{(\gamma+1)M^2 - 2(M^2-1)\sin^2\alpha} - \frac{1}{2M^2\cos^2\alpha}\right], \tag{4.16}$$

$$\left.\frac{\partial\delta_1}{\partial p_2}\right|_{\eta'=0} = \frac{\psi(p_1,\mu)^{\frac{1}{2}}}{\gamma p_1} \frac{\left([2/(\gamma-1)]\left(1 - \frac{1}{2}(\gamma+1)\psi(p_1,\mu)\right)\sin^2\alpha + M^2\right)^{\frac{1}{2}}}{[2/(\gamma-1)]\left(\psi(p_1,\mu) - 1\right)\sin^2\alpha + M^2} \sin\alpha, \tag{4.17}$$

$$\left.\frac{\partial\Gamma'}{\partial\eta'}\right|_{\eta'=0} = \frac{-\gamma^{\frac{1}{2}}}{(\gamma-1)} \frac{1 - \psi(p_1,\mu)}{\left(M^2 + [2/(\gamma-1)]\left(1 - \psi(p_1,\mu)\right)\sin^2\alpha\right)^{\frac{1}{2}}} \frac{\sin 2\alpha}{\cos(\alpha - \delta_0)}, \tag{4.18}$$

$$\left.\frac{\partial\Gamma'}{\partial p_2}\right|_{\eta'=0} = \frac{\gamma^{\frac{1}{2}}}{2(\gamma-1)} \frac{\psi'(1)\psi(p_1,\mu)/p_1 - \psi'(p_1,\mu)}{\left(M^2 + [2/(\gamma-1)]\left(1 - \psi(p_1,\mu)\right)\sin^2\alpha\right)^{\frac{1}{2}}} \frac{\sin 2\alpha}{\cos(\alpha - \delta_0)}, \tag{4.19}$$

where ψ' is the derivative of ψ with respect to the first argument. In figure 14 we plot Γ', the leading term in (4.13), and results from DNS quantification ($\hat{\Gamma}'$), for three Mach numbers ($M = 1.05, 1.5, 4.0$) for an interface inclined at $\alpha = 45°$. Although the circulation was expressed as a series assuming that $1 - \eta^{-\frac{1}{2}}$ is small, we observe that the leading term captures most of the circulation for a large range in η. Note that for $M = 4.0$ the refraction is not regular for $\eta > 5.52$ and hence the exact

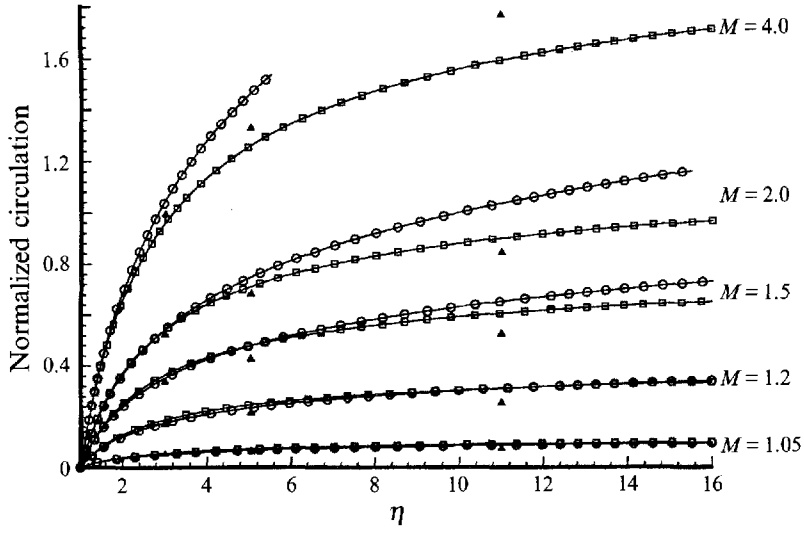

FIGURE 14. Circulation per unit *original* length as a function of η. The angle of the interface is $\alpha = 45°$. The Mach number of the incident shock is indicated in the figure. ○, Γ'; □, leading term in series of Γ' in $1-\eta^{-\frac{1}{2}}$; ▲, $\hat{\Gamma}'$.

circulation shown by the circles terminates. The authors acknowledge the fact that the expression for the leading term is analytically complicated and does not motivate physical insight.

4.4. *Proposed scaling laws*

The above analysis is summarized in the dominant terms for Γ' as

$$\Gamma'_* = \frac{2\gamma^{\frac{1}{2}}}{\gamma+1}(1-\eta^{-\frac{1}{2}})\sin\alpha(1+M^{-1}+2M^{-2})(M-1). \tag{4.20}$$

Equation (4.20) shows that the circulation per unit original length, Γ', scales as

(i) $(1+M^{-1}+2M^{-2})(M-1)$ in Mach number. This leads to linear behaviour in M for large M;

(ii) $(1-\eta^{-\frac{1}{2}})$ for the density ratio. Note that for large η circulation is essentially independent of the density ratio. For $\eta \to \infty$ the circulation should correspond to the slip velocity at a solid surface;

(iii) $(\sin\alpha)$ for the inclination of the interface with the shock;

(iv) $\gamma^{\frac{1}{2}}/(\gamma+1)$ for the ratio of specific heats.

Figure 15 shows the exact circulation, Γ', in the $(M^{-1},\eta^{-\frac{1}{2}})$ plane for $\gamma = 1.4$. The extent of the plane encompasses very weak shocks ($M^{-1} \to 1$) and extremely strong ones ($M^{-1} \to 0$). The density ratio varies from the extremely small ($\eta^{-\frac{1}{2}} \to 1$) to the very large ($\eta^{-\frac{1}{2}} \to 0$). The angle of the interface is $\alpha = 15°, 30°, 45°, 60°$. The normalized circulation is set to zero (white space indicated by IR) where the shock refraction is not RRR. At $\alpha = 60°$ there is a region of RRE indicated by IR in the lower right part of the diagram. Where the scaling law holds exactly the normalized circulation should be exactly equal to one. We define, arbitrarily, the contour levels of 1.1 and 0.9 to be the boundaries where the scaling laws hold. These boundaries correspond to a 10% error (light grey space). Not surprisingly, the domain of applicability shrinks as α increases. For small α, there are regions where the scaling

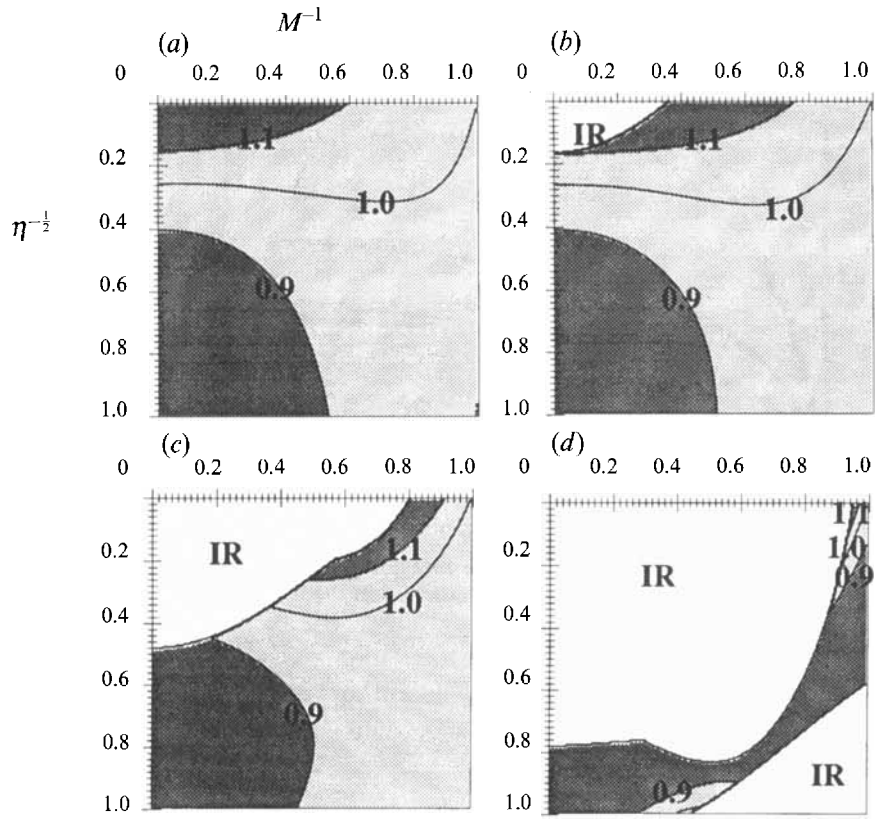

FIGURE 15. Images of circulation per unit unshocked length, Γ', normalized by Γ'_* in the $(M^{-1}, \eta^{-\frac{1}{2}})$ plane. The angle of the interface is (*a*) $\alpha = 15°$; (*b*) $\alpha = 30°$; (*c*) $\alpha = 45°$; (*d*) $\alpha = 60°$. The light (dark) grey areas show where Γ'_* is smaller (larger) than $\pm 10\%$ than Γ'. The white space shows regions where refraction is not RRR.

laws are within the specified error bounds up to very large M at intermediate values of η; and up to very large η at low to moderate values of M. For instance, for $\alpha \leqslant 30°$, the error is less than 10% for $1.0 < M \leqslant 1.32$ for all η, and $5.8 \leqslant \eta \leqslant 32.6$ for all M. Another observation concerns the transition from RRR to IR. Note that for $\alpha = 60°, \eta^{-\frac{1}{2}} = 0.8$, as M increases we proceed from RRR to IR and then back to RRR.

5. Circulation for non-planar interfaces

Hitherto, we have only considered planar interfaces and derived scaling laws for those. In this section, we present analytical expressions for circulation on non-planar interfaces. Consider a non-planar fast–slow interface described by $x = f(y)$ where $f(y)$ and $f^{-1}(y)$ are single valued. In §2, we derived an approximate expression for circulation (2.12) which is of the form

$$\frac{\mathrm{d}\tilde{\Gamma}_3}{\mathrm{d}s} = \Gamma'_1 \sin\alpha + \Gamma'_3 \sin^3\alpha, \tag{5.1}$$

where Γ_1' and Γ_3' depend only upon M, η, γ_0 and γ_b. Integrate equation (5.1) to get the total circulation magnitude on the interface as

$$\tilde{\Gamma}_3 = \tilde{\Gamma}_1 + \Gamma_3' \int_0^{\Delta X} \frac{\mathrm{d}x}{1 + (\mathrm{d}x/\mathrm{d}y)^2}, \tag{5.2}$$

where ΔX (see figure 1) is the range of the interface in the x-direction and $\tilde{\Gamma}_1 = \Gamma_1' \Delta X$ is the total circulation magnitude to first order. The vorticity distribution is given by

$$\tilde{\omega}(x, y) = -\left(\Gamma_1' + \Gamma_3' \frac{f'^2(y)}{1 + f'^2(y)}\right) f'(y) \delta(x - f(y)). \tag{5.3}$$

As examples of non-planar interfaces we consider sinusoidal interfaces and cylindrical bubbles.

5.1. *Sinusoidal interface*

5.1.1. *Circulation on sinusoidal interfaces*

The equation of the interface is $x = x_0 + A \cos ky$. See figure 1(*b*) for a schematic of the interface. Here $k = 2\pi/\lambda$ is the wavenumber. Using (5.2), $\tilde{\Gamma}_3$ on one half-wavelength sinusoidal interface is given by

$$\frac{\tilde{\Gamma}_3}{2A} = \Gamma_1' + \Gamma_3' - \Gamma_3' \frac{1}{2kA(1 + k^2A^2)^{\frac{1}{2}}} \log \left[\frac{(1 + k^2A^2)^{\frac{1}{2}} + kA}{(1 + k^2A^2)^{\frac{1}{2}} - kA}\right]. \tag{5.4}$$

Integrating (5.3) along the x-direction and retaining only the first-order term, we get

$$\int_{-\infty}^{\infty} \tilde{\omega}(x, y) \mathrm{d}x = \tilde{\Omega}(y) = \Gamma_1' Ak \sin ky. \tag{5.5}$$

We conducted several numerical experiments with $A = 16$, $\lambda = 160$ on a 400×80 grid with $\Delta x = \Delta y = 1.0$. We simulate only half the wavelength and stop the calculation when the shock has traversed the interface completely. The largest angle between the shock and the interface occurs at $(0, -\lambda/4)$ and is given by $\tan \alpha_{max} = Ak$. For $A/\lambda = 0.1, \alpha_{max} = 32°$ and the refraction of the shock at the interface is regular at all times; while for $A/\lambda = 0.5, \alpha_{max} = 72°$, for which the refraction is irregular.

Implicit in (5.3) is the fact that the vorticity is distributed on a set of measure zero in the Lebesgue sense. However, in DNS we have a vortex layer. We observe good agreement between DNS results ($\hat{\Omega}(y)$) and the analytical result ($\tilde{\Omega}(y)$) of the x-integrated vorticity for an Air–R22 interface ($A/\lambda = 0.1$) for several Mach numbers (figure 16).

We also observe good agreement between the total circulation, $\tilde{\Gamma}_3$, and $\hat{\Gamma}$ (DNS results) normalized by $\tilde{\Gamma}_1 = 2A\Gamma_1'$ (figure 17). Note that the magnitude of Γ_1' may be obtained from figure 7. The agreement worsens as A/λ increases. As before, one source of discrepancy between the analytical and numerical results is that the time taken for the shock to traverse the interface is large for large A/λ ratios and the vortex layer evolves during this time. From our DNS we observe that, at later times, the vorticity on the interface coalesces to form a mushroom-shaped coherent structure. At this later time, the vorticity distribution is no longer governed by (5.3); however, the total circulation remains close to that predicted by (5.4). We are developing an analytical *incompressible* vortex paradigm for the growth rate of a single mode and will present it in a future publication.

For the sake of completeness, we briefly mention an investigation of the *slow–fast*

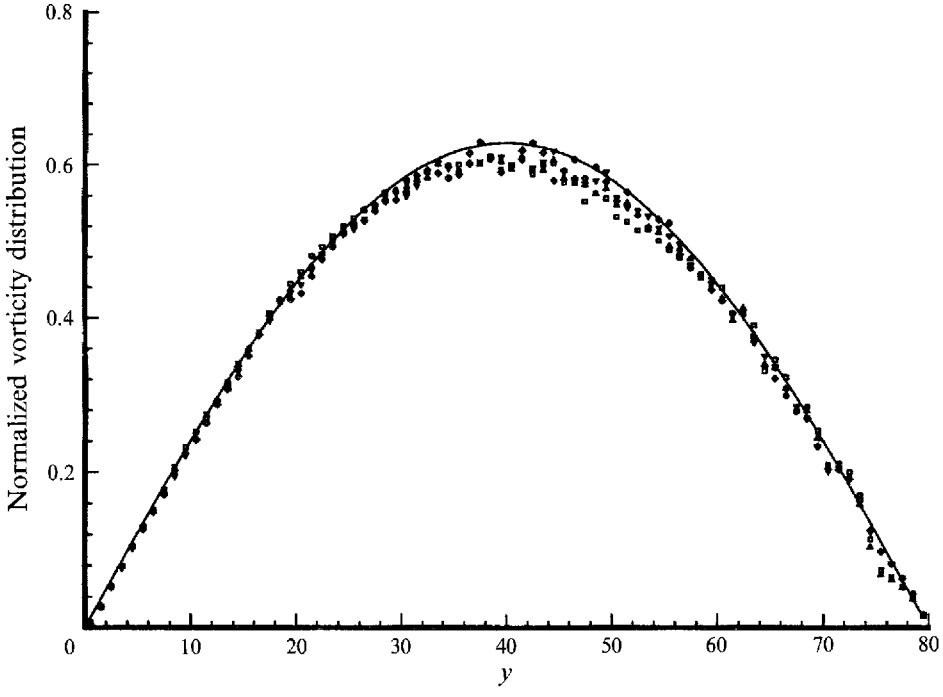

FIGURE 16. Magnitude of vorticity distribution normalized by $2A\Gamma_1'$ as a function of y for a sinusoidal Air–R22 interface ($A/\lambda = 0.1$). The solid line is the analytical result $\tilde{\Omega}(y)$. The symbols correspond to $\hat{\Omega}(y)$. The Mach numbers of the incident shock are: $M = 1.05(\square), 1.2(\triangle), 1.5(\triangledown), 2.0(\diamond)$.

interaction. Typically, for a slow–fast interface the shock refraction is of the RRE type for small α (Henderson *et al.* 1991). The circulation per unit unshocked length, $\tilde{\Gamma}_{sf}'$, may be expressed as a series in $\sin\alpha$ as

$$\tilde{\Gamma}_{sf}' = \Gamma_{sf}' \sin\alpha + O(\sin^3\alpha), \tag{5.6}$$

where Γ_{sf}' is given by

$$\Gamma_{sf}' = \frac{\gamma_0^{\frac{1}{2}}}{M}\left(\frac{1}{\gamma_b - 1}\frac{1-\psi(p_{20},\mu_b)}{\eta\gamma_0/\gamma_b} - \frac{1}{\gamma_0 - 1}\left(1-\psi(p_1,\mu_0)\left(\frac{p_{20}}{p_1}\right)^{\frac{\gamma_0-1}{\gamma_0}}\right)\right). \tag{5.7}$$

Thus, the total circulation to first order is

$$\tilde{\Gamma}_{sf} = 2A\Gamma_{sf}'. \tag{5.8}$$

In figure 18 we compare the $\tilde{\Gamma}_{sf}/2A$ with results from DNS for an Air–He sinusoidal interface with $A = 16$ and $\lambda = 160$. The transition to irregularity takes place at smaller angles and thus the difference between the analytical result and DNS is larger than for the fast–slow cases. Obviously, higher-order terms are necessary in the above series expansion.

5.2. *Circular interfaces*

In figure 19 we show images of (*a*) vorticity and (*b*) numerical shadowgraphs of DNS of an Air–R22 shock–bubble interaction for $M = 1.5$. Time increases from left to right in each row. The numerical experiments were done on a 400×80 grid with $\Delta x = \Delta y = 1.0$ and $r_0 = 50$. We divide the vorticity deposition into three phases:

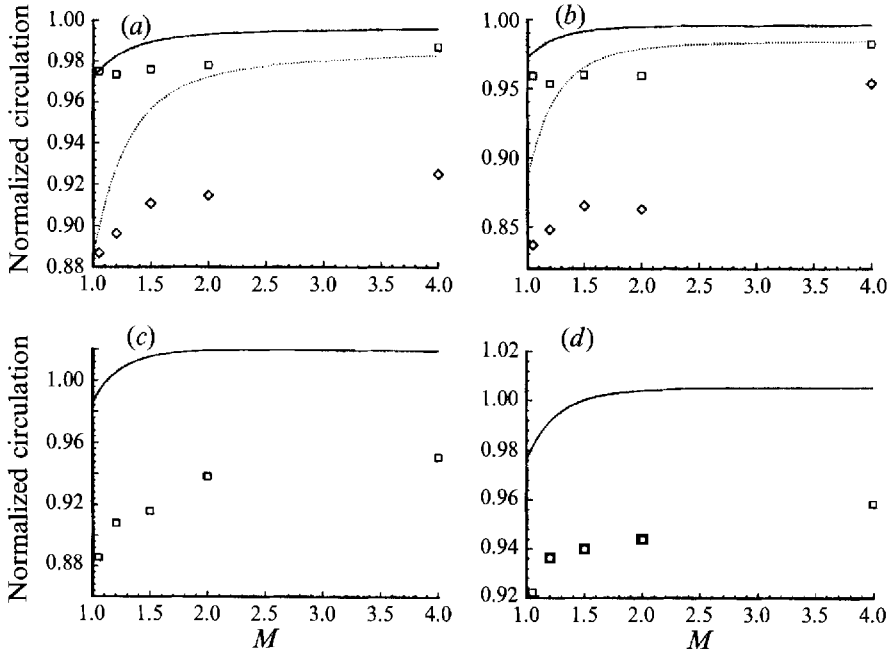

FIGURE 17. Total circulation magnitude normalized by $\tilde{\Gamma}_1' = 2A\Gamma_1'$ for a sinusoidal interface given by $x = x_0 + A\cos ky$. The solid (dotted) line is $\tilde{\Gamma}_3/(2A\Gamma_1')$ for $A/\lambda = 0.1$ ($A/\lambda = 0.5$). The interfaces are (*a*) Air–R22; (*b*) Air–SF_6; (*c*) He–CO_2; and (*d*) He–Xe. □ (◇), $\hat{\Gamma}/(2A\Gamma_1')$ for $A/\lambda = 0.1$ ($A/\lambda = 0.5$).

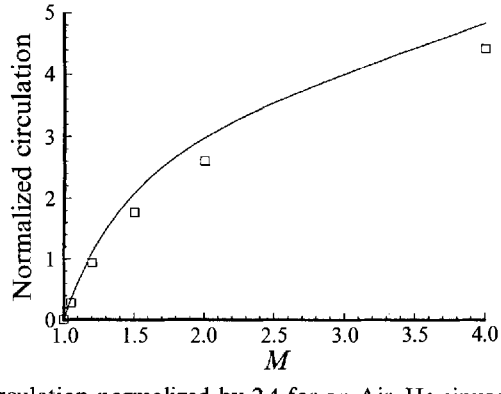

FIGURE 18. Total circulation normalized by $2A$ for an Air–He sinusoidal interface given by $x = x_0 + A\cos ky$. The solid line is $\tilde{\Gamma}_{sf}/2A$ and □, $\hat{\Gamma}_{sf}/(2A)$ for $A/\lambda = 0.1$.

Phase (i): During this phase the shock undergoes regular refraction at the bubble interface. The shock polar equations are valid in this phase. This phase ends when the shock polar equations break down at a certain critical angle (first left image in figure 19).

Phase (ii): This phase lasts until the shock is at the top of the bubble, i.e. $\alpha = \pi/2$ (second frame in figure 19).

Phase (iii): As the shock moves over the top of the bubble, it curves back to

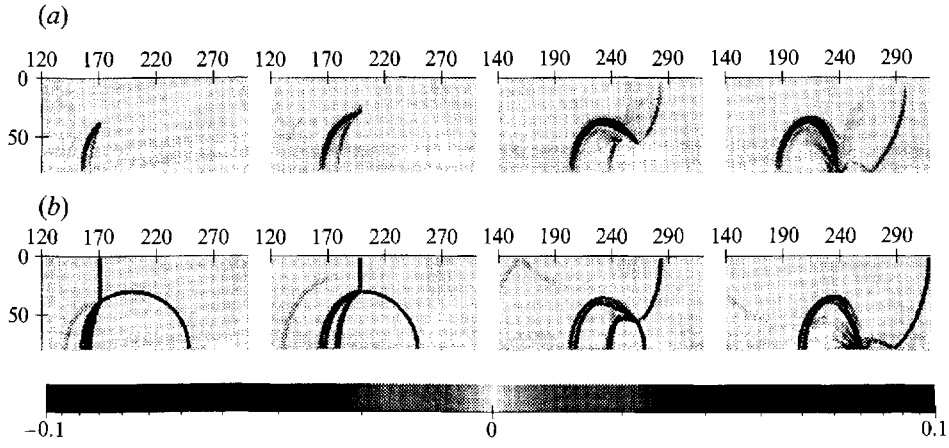

FIGURE 19. (*a*) Vorticity and (*b*) numerical shadowgraphs for an Air–R22 shock bubble interaction. $M = 1.5$.

meet the interface (third frame in figure 19). However, for weak incident shocks, weak compression waves touch the interface and continue into the bubble where they coalesce to form a shock. Phase (iii) ends when the primary shock reflects off the lower boundary and deposits opposite-signed vorticity on the interface (fourth frame in figure 19).

5.2.1. *Circulation at the end of phase (ii)*

We use (5.2) to get the circulation on the 'uside' of the bubble (see figure 1*c*) which satisfies the conditions that the equation for the interface be a single-valued function of y. The circulation magnitude on the 'uside' of the bubble, to first and third order, is

$$\tilde{\Gamma}_1 = \Gamma_1' r_0, \tag{5.9}$$

$$\tilde{\Gamma}_3 = \Gamma_1' r_0 + \tfrac{2}{3}\Gamma_3' r_0. \tag{5.10}$$

In figure 20 we plot $\tilde{\Gamma}_3/\tilde{\Gamma}_1$ as a function of Mach number, M, for the following interfaces: Air–R22, Air–SF_6 He–CO_2 and He–Xe. The symbols in the figure indicate quantification from DNS ($\hat{\Gamma}/\tilde{\Gamma}_1$). This example illustrates an interface where we have rapid traversal of the interface and where the angle between the shock and the interface varies continuously from 0 to $\pi/2$. The agreement between the analysis and DNS is very good, especially for lower density ratios. The third-order contribution to the total circulation is small for most cases.

5.2.2. *Total circulation at the end of phase (iii)*

The above analytical result gives us the total circulation on the bubble when the shock is on top of the bubble. As the shock diffracts over the bubble surface, the phenomenon gets complicated. Eventually, the vortex layer on the bubble surface rolls up to form a coherent vortex. It is important to quantify the strength of this vortex structure. Figure 21 shows the space–time diagram of the baroclinic source term, i.e. $\int(\nabla\rho\times\nabla p)/\rho^2 \mathrm{d}y$, for an $M = 1.5$ shock interacting with an Air–R22 circular interface. In figure 21, we clearly see that the primary shock curves backwards to contact the interface; at $t \approx 80$ we see another dominant black streak to the left of the main black streak; this is caused by the refraction of the transmitted shock with

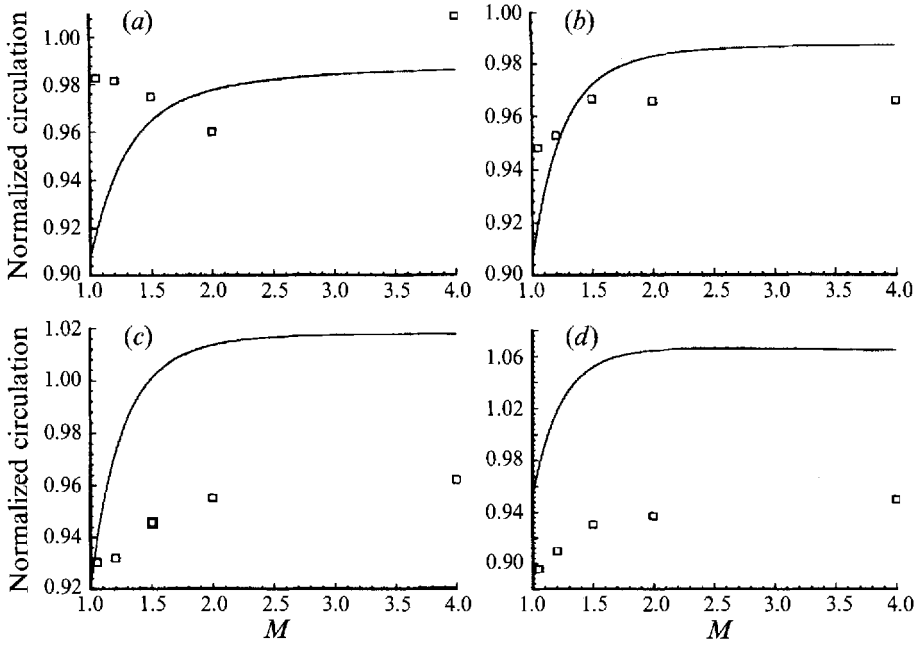

FIGURE 20. Total circulation magnitude at the end of phase (ii) normalized by $\tilde{\Gamma}_1' r_0$ for a cylindrical bubble. The interfaces are (*a*) Air–R22; (*b*) Air–SF_6; (*c*) He–CO_2; and (*d*) He–Xe. The solid line is $\tilde{\Gamma}_3/(\Gamma_1' r_0)$. □, $\hat{\Gamma}/(\Gamma_1' r_0)$.

the interface. At $t \approx 100$ we see the appearance of a white streak which indicates the reflection of the shock and deposition of opposite-signed vorticity on the interface. For larger density ratio cases such as He–CO_2 or He–Xe interfaces, the transmitted shock reaches the 'dside' of the bubble (see figure 1*c*) fairly late and deposits vorticity of the same sign as in the primary interaction. Let $\tilde{\Gamma}_{iii}$ refer to the circulation on the interface at the end of phase (iii). We adopt the so-called 'visiometric' approach (Silver & Zabusky, 1992) to model $\tilde{\Gamma}_{iii}$. The complicated phenomenon at the back side of the bubble are all lumped together in a 'near-normality' hypothesis which is: the primary density and the pressure gradients are nearly perpendicular to each other. The basis of this hypothesis is the visual inspection of numerous numerical shadowgraphs.

We also investigated the validity of the 'near-normality' hypothesis using geometrical shock dynamics (Henshaw, Smyth & Schwendeman 1986; Schwendeman 1988) and found the angle between the shock and the interface to be $\pi/2 \pm \pi/12$ after phase (ii) for the parameter space discussed here. Since the sine of the angle is used in the model, the error is small. Note that in geometrical shock dynamics the angle between the shock and the interface after phase (ii) is exactly $\pi/2$ if $\eta \to \infty$. This 'near-normality' assumption is violated if $\eta \approx 1$. Retaining terms up the third order, we get

$$\tilde{\Gamma}_{iii} = (1 + \tfrac{1}{2}\pi)\Gamma_1' r_0 + (\tfrac{2}{3} + \tfrac{1}{2}\pi)\Gamma_3' r_0. \tag{5.11}$$

Retaining only the first-order term in (5.2) we get

$$\tilde{\Gamma}_{iii} = (1 + \tfrac{1}{2}\pi)\Gamma_1' r_0. \tag{5.12}$$

We abbreviate our model as SZ1.

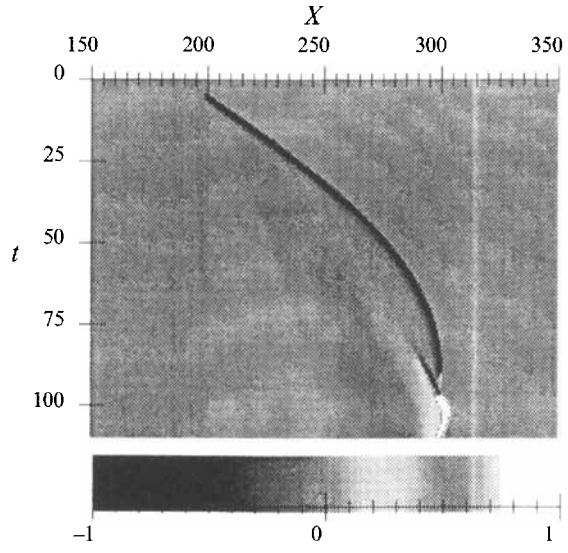

FIGURE 21. Space–time diagram of y-integrated baroclinic source term for an Air–R22 shock–bubble interaction for $M = 1.5$.

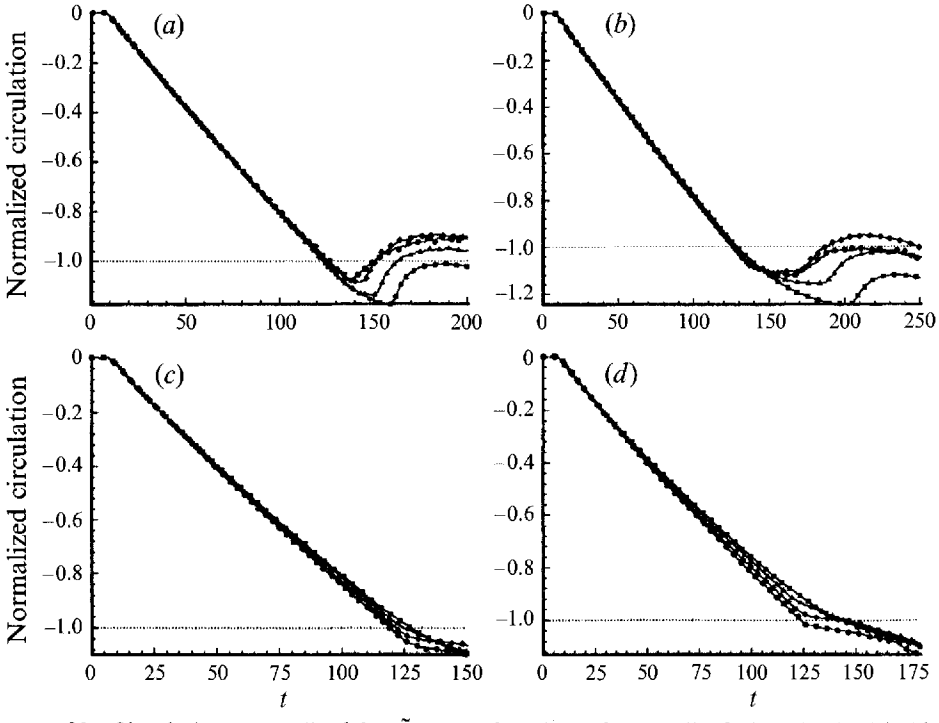

FIGURE 22. Circulation normalized by $\tilde{\Gamma}_{iii}$ as a function of normalized time (tM). (*a*) Air–R22; (*b*) Air–SF_6; (*c*) He–CO_2; (*d*) He–Xe. The dotted line shows the analytical result. In each case $M = 1.05, 1.2, 1.5, 2.0$.

In figure 22 we plot the circulation from DNS normalized by $\tilde{\Gamma}_{iii}$, (5.12). The time axis is normalized by M. We observe that the curves for different M collapse indicating that the scaling chosen is very good. For very large density ratio cases after phase (ii) the different curves seem to depart from each other. The end of phase (ii) is at $t = 50.28$ for Air–R22 and Air–SF_6 interfaces, and at $t = 46.08$ for He–CO_2 and He–Xe interfaces. The end of phase (iii) is apparent in most cases as the first kink. For the Air–R22 and Air–SF6 interfaces, the difference between $\tilde{\Gamma}_{iii}$ and DNS results at the end of phase (iii) seem larger because the transmitted shock is also contributing to the circulation. In our numerical experiments, we noticed that the circulation for the larger density ratios increases with time due to secondary effects which are not explained by our model.

5.3. *Comparison of models*

5.3.1. *Picone–Boris model*

The model proposed by Picone & Boris (1983) and Picone *et al.* (1988) (PB) may be written in our notation as

$$\Gamma_{iii} = \frac{4\gamma^{\frac{1}{2}}}{\gamma+1}\frac{M^2-1}{M}\frac{\gamma M^2+1}{(\gamma+1)M^2}\log(\eta)r_0. \tag{5.13}$$

This model was derived for both the s/f and the f/s shock–bubble interactions. The weaknesses of this model are that it is not asymptotically motivated and assumes fore and aft symmetry ($\Gamma_{ii} = 0.5\Gamma_{iii}$), and that the circulation is not bounded and diverges logarithmically as $\eta \to \infty$.

5.3.2. *Rudinger–Sommers model*

Rudinger & Sommers (1960) proposed a model (RS) for the strength of the vortex as

$$\Gamma_{iii} = \frac{4\gamma^{\frac{1}{2}}}{\gamma+1}\frac{M^2-1}{M}\frac{\eta-1}{\eta+1}r_0. \tag{5.14}$$

5.3.3. *Scaling law model*

In §4 scaling laws were derived for circulation per unit *unshocked* length of the interface. Integrating (4.20) from $\alpha = 0$ to $\alpha = \pi/2$ and using the near-normality hypothesis, leads to the simplest asymptotically motivated model for circulation (abbreviated SZ2) in f/s shock–bubble interactions:

$$\Gamma_{iii} = \left(1+\frac{\pi}{2}\right)\frac{2\gamma^{\frac{1}{2}}}{\gamma+1}(1-\eta^{-\frac{1}{2}})(1+M^{-1}+2M^{-2})(M-1)r_0. \tag{5.15}$$

5.3.4. *Discussion*

None of the models discussed in this sub-section considered the change in ratio of specific heats across the interface although certain corrections were proposed by Picone–Boris and Rudinger–Sommers. For comparison with DNS we use the same ratio of specific heats, $\gamma = 1.4$, in both gases and use $\eta = 3.0, 6.0, 15.0$ interfaces. The total circulation at the end of phase (iii) normalized by r_0 is plotted in figures 23(*a–c*) for all the models. Note that the Picone–Boris model (PB) agrees for smaller density ratios due to a fortuitous cancellation of errors, and overpredicts for larger η. The Rudinger–Sommers model (RS) underpredicts especially for larger Mach numbers. Both our models, SZ1 and SZ2, agree well with DNS results and with each other.

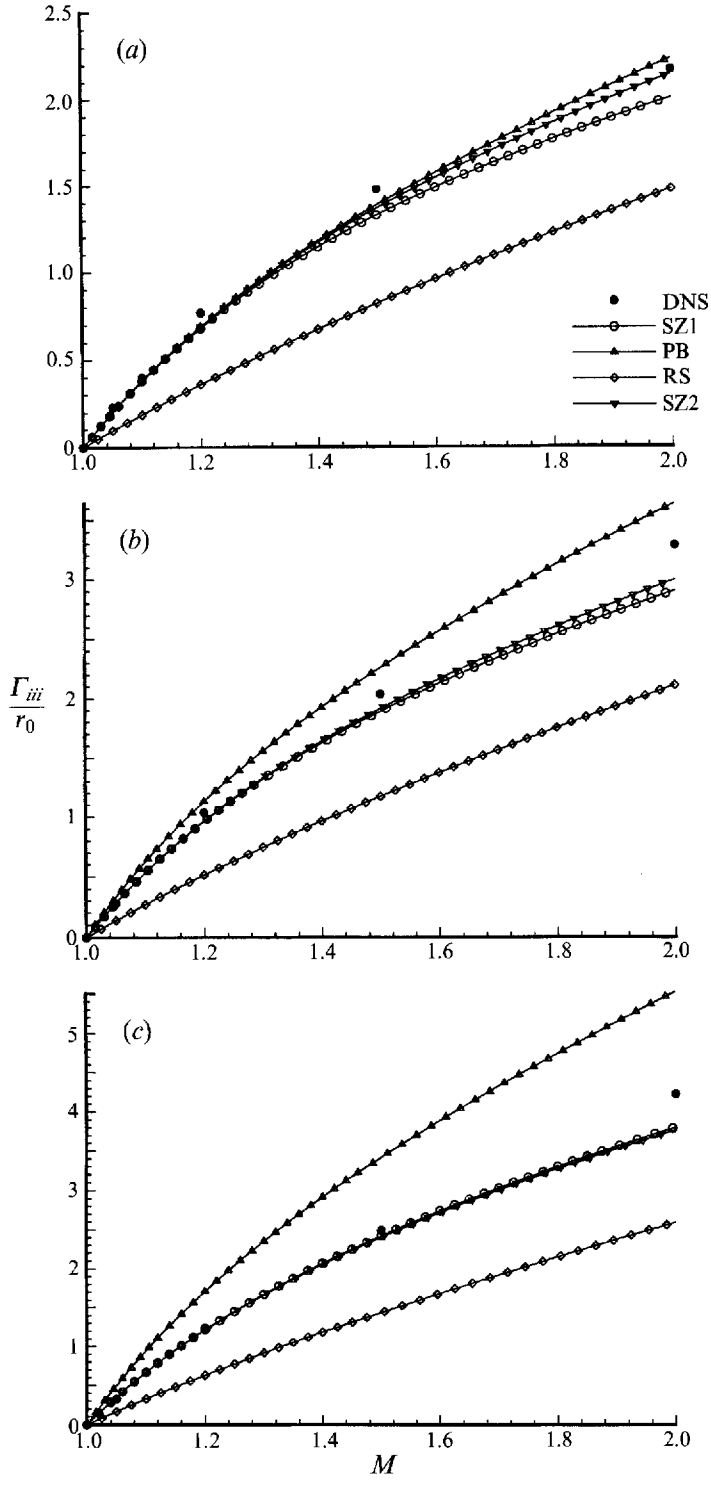

FIGURE 23. Comparison of DNS with models for circulation in shock-bubble interactions as a function of Mach number for (*a*) an $\eta = 3$ interface; (*b*) an $\eta = 6$ interface; (*c*) an $\eta = 15$ interface.

Note that the SZ2 model gives the dependence on various quantities explicitly and is the simplest model.

6. Conclusion and future work

One of the primary objectives of this work was to quantify the baroclinic vorticity generation in Richtmyer–Meshkov environments. An analytical expression, based on shock polar analysis, was derived for circulation on f/s planar interfaces. This expression was valid only for regular refraction (RRR) of shock waves. An approximate expression for circulation, based on truncated series expansions in $\sin\alpha$, was derived which can be used for irregular refractions of the shock. A comparison within RRR showed that the first-order term captures most of the circulation. It was also shown that the third-order term contributes negligibly for Mach numbers $M \geqslant 1.5$. Both the first- and third-order terms were shown to be real for all cases. By a judicious selection of expansion variables, we determined the key result in our paper, namely the scaling laws for circulation on planar interfaces (see (4.20) and figure 15).

We also demonstrated that circulation is a very weak function of changes in ratio of specific heats across the interface. The analytical expressions predict the initial vorticity deposition on the interface, and for large angles are not very useful since the flow field evolution has changed much of the vorticity distribution in the domain.

An analytical expression for circulation on monotonic non-planar interfaces was developed. The analytical expression was confirmed by DNS of the full nonlinear equations for sinusoidal interfaces and the 'uside' of circular bubbles. A model was developed for the total circulation on circular bubbles by hypothesizing the near-normality of the shock with the bubble surface during diffraction.

In the future, we will extend the baroclinic vorticty generation to three-dimensional interfaces. Also, we will model the growth rate of sinusoidally perturbed interfaces in two and three dimensions using vorticity distributions. Effects of compressibility will be quantified.

This work was supported in part by the National Science Foundation, Grant No. DMS-8901900. R.S. was supported by a graduate assistantship from CAIP center, Rutgers University. We acknowledge the Cray-90 computer time provided by the Pittsburgh Supercomputing Center.

Appendix. Derivations

A.1. *Derivation of* Γ'

Let Γ'_s be the circulation per unit *shocked* length of the interface. Then Γ'_s is given by

$$\Gamma'_s \equiv v_t - v_2, \tag{A 1}$$

and

$$v_2 = M_2 c_2, \quad v_t = M_t c_t. \tag{A 2}$$

The Mach number behind the transmitted wave, M_t is given by

$$\frac{1 + \frac{1}{2}(\gamma_b - 1)M_b^2}{1 + \frac{1}{2}(\gamma_b - 1)M_t^2} = \psi(p_2/p_0, \mu_b), \tag{A 3}$$

or

$$M_t = \left(\frac{2}{\gamma_b - 1}\right)^{\frac{1}{2}} \left[\frac{1}{\psi(p_2/p_0, \mu_b)} \left\{1 + \frac{\gamma_b - 1}{2} \frac{M^2}{\sin^2\alpha} \eta \frac{\gamma_0}{\gamma_b}\right\} - 1\right]^{\frac{1}{2}}. \tag{A 4}$$

The sound speed behind the transmitted shock is given by

$$c_t^2 = \frac{\gamma_b p_2}{\rho_t} = \left(\frac{\gamma_0 p_0}{\rho_0}\right)\left(\frac{p_2}{p_0}\right)\left(\frac{\rho_b}{\rho_t}\right)\left(\frac{\gamma_b}{\gamma_0 \eta}\right), \tag{A 5}$$

where ρ_t is the density behind the transmitted shock. Using the Rankine–Hugoniot jump conditions, express ρ_b/ρ_t as a function of p_2/p_0. This gives,

$$c_t^2 = \left(\frac{\gamma_0 p_0}{\rho_0}\right)\left(\frac{\gamma_b}{\gamma_0 \eta}\right)\psi(p_2/p_0, \mu_b). \tag{A 6}$$

The tangential velocity, v_t is then

$$v_t = M_t c_t = \left(\frac{\gamma_0 p_0}{\rho_0}\right)^{\frac{1}{2}} \frac{1}{\sin\alpha} \left[M^2 + \frac{2}{\gamma_b - 1}\left(\frac{1 - \psi(p_2, \mu_b)}{\eta\gamma_0/\gamma_b}\right)\sin^2\alpha\right]^{\frac{1}{2}}. \tag{A 7}$$

The Mach number, M_2, behind the reflected shock is given by

$$\frac{1 + \frac{1}{2}(\gamma_0 - 1)M_1^2}{1 + \frac{1}{2}(\gamma_0 - 1)M_2^2} = \psi(p_2/p_1, \mu_0). \tag{A 8}$$

The Mach number, M_1, behind the incident shock is given by

$$\frac{1 + \frac{1}{2}(\gamma_0 - 1)M_0^2}{1 + \frac{1}{2}(\gamma_0 - 1)M_1^2} = \psi(p_1/p_0, \mu_0). \tag{A 9}$$

Therefore,

$$M_2 = \left(\frac{2}{\gamma_0 - 1}\right)^{\frac{1}{2}} \left[\frac{1}{\psi(p_2/p_1, \mu_0)\psi(p_1/p_0, \mu_0)} \left\{1 + \frac{\gamma_0 - 1}{2} \frac{M^2}{\sin^2\alpha}\right\} - 1\right]^{\frac{1}{2}}. \tag{A 10}$$

The sound speed behind the reflected shock is given by

$$c_2^2 = \frac{\gamma_0 p_2}{\rho_b} = \left(\frac{\gamma_0 p_0}{\rho_0}\right)\left(\frac{p_2}{p_1}\right)\left(\frac{p_1}{p_0}\right)\left(\frac{\rho_1}{\rho_2}\right)\left(\frac{\rho_0}{\rho_1}\right), \tag{A 11}$$

where ρ_2 is the density behind the reflected shock. Using the Rankine–Hugoniot jump conditions, express ρ_1/ρ_2 and ρ_0/ρ_1 as functions of p_2/p_1 and p_1/p_0 respectively This gives,

$$c_2^2 = \left(\frac{\gamma_0 p_0}{\rho_0}\right)\psi(p_2/p_1, \mu_0)\psi(p_1/p_0, \mu_0). \tag{A 12}$$

Thus the tangential velocity, v_2 is given by

$$\begin{aligned} v_2 &= M_2\, c_2 \\ &= \left(\frac{\gamma_0 p_0}{\rho_0}\right)^{\frac{1}{2}} \frac{1}{\sin\alpha} \left[M^2 + \frac{2}{\gamma_0 - 1}\left(1 - \psi(p_2/p_1, \mu_0)\psi(p_1/p_0, \mu_0)\right)\sin^2\alpha\right]^{\frac{1}{2}}. \end{aligned} \tag{A 13}$$

We have normalized $p_0 = \rho_0 = 1$. The difference $v_t - v_2$ multiplied by the geometric factor $\mathrm{d}s'/\mathrm{d}s = [\cos\alpha/\cos(\alpha - \delta_b)]$ gives the circulation per unit *unshocked* length as given in (2.11).

A.2. *Derivation of* Γ_3'

The circulation per unit length of the *shocked* interface is essentially a function of α and p_2. Let Γ_s' be the circulation per unit *shocked* length of the interface. Expressing Γ_s' as a double Taylor series we get

$$\begin{aligned}\Gamma_s' = {} & \frac{\partial \Gamma_s'}{\partial \sin\alpha}\bigg|_{\sin\alpha=0} \sin\alpha + \frac{\partial \Gamma_s'}{\partial p_2}\bigg|_{\sin\alpha=0} (p_2 - p_{20}) \\ & + \frac{1}{2}\frac{\partial^2 \Gamma_s'}{\partial \sin^2\alpha}\bigg|_{\sin\alpha=0} \sin^2\alpha + \frac{\partial^2 \Gamma_s'}{\partial \sin\alpha \partial p_2}\bigg|_{\sin\alpha=0} (p_2 - p_{20})\sin\alpha \\ & + \frac{1}{2}\frac{\partial^2 \Gamma_s'}{\partial p_2^2}\bigg|_{\sin\alpha=0} (p_2 - p_{20})^2 + \frac{1}{3!}\frac{\partial^3 \Gamma_s'}{\partial \sin^3\alpha}\bigg|_{\sin\alpha=0} \sin^3\alpha + \cdots. \end{aligned} \tag{A 14}$$

To get the circulation per unit length of the original interface, we multiply Γ_s' by the length correction factor given by

$$\phi = \frac{\cos\alpha}{\cos(\alpha - \delta_b)}. \tag{A 15}$$

Expressing the length correction factor as a series in $\sin\alpha$ and using the fact that it is an even function of $\sin\alpha$, we get

$$\phi = 1 + \frac{1}{2}\frac{\partial^2 \phi}{\partial \sin^2\alpha}\bigg|_{\sin\alpha=0} \sin^2\alpha + \frac{\partial \phi}{\partial p_2}\bigg|_{\sin\alpha=0} (p_2 - p_{20}) + O(\sin^4\alpha), \tag{A 16}$$

$$\frac{\partial \phi}{\partial p_2}\bigg|_{\sin\alpha=0} = 0. \tag{A 17}$$

The term $(p_2 - p_{20})$ is obtained by expressing (2.7) as a series in $\sin\alpha$:

$$\begin{aligned} & \frac{\partial \delta_0(p_1)}{\partial \sin\alpha}\bigg|_{\sin\alpha=0} \sin\alpha + \frac{1}{3!}\frac{\partial^3 \delta_0(p_1)}{\partial \sin^3\alpha}\bigg|_{\sin\alpha=0} \sin^3\alpha + O(\sin^5\alpha) \\ & = \frac{\partial \delta_1(p_2/p_1)}{\partial \sin\alpha}\bigg|_{\sin\alpha=0} \sin\alpha + \frac{1}{3!}\frac{\partial^3 \delta_1(p_2/p_1)}{\partial \sin^3\alpha}\bigg|_{\sin\alpha=0} \sin^3\alpha \\ & \quad + \frac{\partial^2 \delta_1(p_2/p_1)}{\partial p_2 \partial \sin\alpha}\bigg|_{\sin\alpha=0} (p_2 - p_{20})\sin\alpha + \frac{\partial \delta_b(p_2)}{\partial \sin\alpha}\bigg|_{\sin\alpha=0} \sin\alpha \\ & \quad + \frac{1}{3!}\frac{\partial^3 \delta_b(p_2)}{\partial \sin^3\alpha}\bigg|_{\sin\alpha=0} \sin^3\alpha + \frac{\partial^2 \delta_b(p_2)}{\partial p_2 \partial \sin\alpha}\bigg|_{\sin\alpha=0} (p_2 - p_{20})\sin\alpha \\ & \quad + O(\sin^5\alpha). \end{aligned} \tag{A 18}$$

Equating coefficients of the leading-order term gives (2.15). Equating the third-order coefficient gives the leading term in the $\sin\alpha$ series of p_2. Thus we get

$$\begin{aligned} p_2 - p_{20} = {} & \frac{\dfrac{1}{3!}\dfrac{\partial^3 \delta_0(p_1)}{\partial \sin^3\alpha}\bigg|_{\sin\alpha=0} - \dfrac{1}{3!}\dfrac{\partial^3 \delta_b(p_2)}{\partial \sin^3\alpha}\bigg|_{\sin\alpha=0} - \dfrac{1}{3!}\dfrac{\partial^3 \delta_1(p_2/p_1)}{\partial \sin^3\alpha}\bigg|_{\sin\alpha=0}}{\dfrac{\partial^2 \delta_b(p_2)}{\partial p_2 \partial \sin\alpha}\bigg|_{\sin\alpha=0} + \dfrac{\partial^2 \delta_1(p_2/p_1)}{\partial p_2 \partial \sin\alpha}\bigg|_{\sin\alpha=0}} \sin^2\alpha \\ & + O(\sin^4\alpha). \end{aligned} \tag{A 19}$$

Collecting terms of order $\sin^3\alpha$ in Γ' gives

$$\Gamma_3' = \left[\frac{\partial \Gamma_s'}{\partial \sin\alpha}\bigg|_{\sin\alpha=0}\right]\left[\frac{1}{2}\frac{\partial^2\phi}{\partial \sin^2\alpha}\bigg|_{\sin\alpha=0}\right] + \left[\frac{\partial^2\Gamma_s'}{\partial \sin\alpha \partial p_2}\bigg|_{\sin\alpha=0}\right] \times \left[\frac{\frac{1}{3!}\frac{\partial^3\delta_0(p_1)}{\partial \sin^3\alpha}\Big|_{\sin\alpha=0} - \frac{1}{3!}\frac{\partial^3\delta_b(p_2)}{\partial \sin^3\alpha}\Big|_{\sin\alpha=0} - \frac{1}{3!}\frac{\partial^3\delta_1(p_2/p_1)}{\partial \sin^3\alpha}\Big|_{\sin\alpha=0}}{\frac{\partial^2\delta_b(p_2)}{\partial p_2 \partial \sin\alpha}\Big|_{\sin\alpha=0} + \frac{\partial^2\delta_1(p_2/p_1)}{\partial p_2 \partial \sin\alpha}\Big|_{\sin\alpha=0}}\right] + \frac{1}{3!}\frac{\partial^3\Gamma_s'}{\partial \sin^3\alpha}\bigg|_{\sin\alpha=0}. \tag{A 20}$$

After some algebra we obtain the various terms contributing to the third-order term Γ_3':

$$\frac{1}{3!}\frac{\partial^3\Gamma_s'}{\partial \sin^3\alpha}\bigg|_{\sin\alpha=0} = \frac{1}{2\gamma_0^{\frac{3}{2}}M^3}\left[\left(\frac{\gamma_0}{\gamma_0-1}\right)^2\left(1-\psi(p_{20}/p_1,\mu_0)\psi(p_1,\mu_0)\right)^2 - \left(\frac{\gamma_b}{\gamma_b-1}\right)^2\left(\frac{1-\psi(p_{20},\mu_b)}{\eta}\right)^2\right], \tag{A 21}$$

$$\frac{\partial^2\Gamma_s}{\partial p_2 \partial \sin\alpha}\bigg|_{\alpha=0} = -\frac{1}{\gamma_0 M}\left[\left(\frac{\gamma_b}{\gamma_b-1}\right)\frac{\psi'(p_{20},\mu_b)}{\eta} - \left(\frac{\gamma_0}{\gamma_0-1}\right)\psi'(p_{20}/p_1,\mu_0)\frac{\psi(p_1,\mu_0)}{p_1}\right], \tag{A 22}$$

$$\frac{1}{2}\frac{\partial\Gamma_s}{\partial \sin\alpha}\frac{\partial^2\phi}{\partial \sin^2\alpha}\bigg|_{\sin\alpha=0} = -\Gamma_1'\tilde{\phi}\left(1-\tilde{\phi}/2\right), \tag{A 23}$$

where

$$\tilde{\phi} = \frac{(p_{20}-1)(\mu_b^2+1)^{\frac{1}{2}}}{\gamma_b M \eta^{\frac{1}{2}}(\gamma_0/\gamma_b)^{\frac{1}{2}}(\mu_b^2+p_{20})^{\frac{1}{2}}}, \tag{A 24}$$

$$\frac{1}{3!}\frac{\partial^3\delta_0}{\partial \sin^3\alpha}\bigg|_{\sin\alpha=0} = F(p_1-1, M, \gamma_0), \tag{A 25}$$

$$\frac{1}{3!}\frac{\partial^3\delta_b}{\partial \sin^3\alpha}\bigg|_{\sin\alpha=0} = F(p_{20}-1, M\eta^{\frac{1}{2}}(\gamma_0/\gamma_b)^{\frac{1}{2}}, \gamma_b), \tag{A 26}$$

$$\frac{1}{3!}\frac{\partial^3\delta_1}{\partial \sin^3\alpha}\bigg|_{\sin\alpha=0} = F(p_{20}/p_1-1, M/\psi^{\frac{1}{2}}(p_1,\mu_0), \gamma_0) - \frac{1/\gamma_0(\gamma_0-1)(2\gamma_0/\gamma_0+1)^{\frac{1}{2}}1-\psi(p_1,\mu_0)/\psi(p_1,\mu_0)}{M^3/\psi^{\frac{3}{2}}(p_1,\mu_0)} \times \frac{p_{20}/p_1-1}{(\mu_0^2+p_{20}/p_1)^{\frac{1}{2}}}, \tag{A 27}$$

$$\left.\frac{\partial^2 \delta_b}{\partial p_2 \partial \sin\alpha}\right|_{\alpha=0} = G(p_{20}-1, M\eta^{\frac{1}{2}}(\gamma_0/\gamma_b)^{\frac{1}{2}}, \gamma_b), \tag{A 28}$$

$$\left.\frac{\partial^2 \delta_1}{\partial p_2 \partial \sin\alpha}\right|_{\alpha=0} = G(p_{20}/p_1 - 1, M/\psi^{\frac{1}{2}}(p_1, \mu_0), \gamma_0)/p_1, \tag{A 29}$$

$$F(x,y,\gamma) = \frac{x}{y^3}\left[-\frac{1}{2\gamma\beta}(\beta^2+x)^{\frac{1}{2}} + \frac{\beta}{\gamma^2}\frac{x}{(\beta^2+x)^{\frac{1}{2}}} - \frac{1}{3}\frac{\beta^3}{\gamma^3}\frac{x^2}{(\beta^2+x)^{\frac{3}{2}}}\right], \tag{A 30}$$

$$G(x,y,\gamma) = \frac{\beta}{\gamma y}\frac{1}{(\beta^2+x)^{\frac{1}{2}}}\left[1 - \frac{1}{2}\frac{x}{\beta^2+x}\right], \tag{A 31}$$

where

$$\beta^2 = \frac{2\gamma}{\gamma+1} = \mu^2 + 1. \tag{A 32}$$

REFERENCES

ABD-EL-FATTAH, A. M. & HENDERSON, L. F. 1978 Shock waves at a fast-slow gas interface. *J. Fluid Mech.* **86**,15–32.

ARNETT, W. D., BAHCALL, J. N., KIRSHNER, R. P. & WOOSLEY, S. E. 1989 Supernova 1987A. *Ann. Rev. Astron. Astrophys.* **27**, 629.

BITZ, F. & ZABUSKY, N. J. 1990 David and "Visiometrics": visualizing, diagnosing and quantifying evolving amorphous objects. *Comput. Phys.* **4**, 603–614.

COLELLA, P. 1985 A direct Eulerian MUSCL scheme for gas dynamics. *SIAM J. Sci. Stat. Comput.* **6**, 104–117.

GROVE, J. 1989 The interaction of shock waves with fluid interfaces. *Adv. Appl. Maths*, **10**, 201–227.

HAAS, J. F. & STURTEVANT, B. 1987 Interaction of weak shock waves with cylindrical and spherical gas inhomogeneities. *J. Fluid Mech.* 181, 41–76.

HAWLEY, J. F. & ZABUSKY, N. J. 1989 Vortex paradigm for shock-accelerated density-stratified interfaces. *Phys. Rev. Lett.* **63**, 1241–1244.

HENDERSON, L. F. 1966 The refraction of a plane shock wave at a gas interface. *J. Fluid Mech.* **26**, 607–637.

HENDERSON, L. F. 1989 On the refraction of shock waves. *J. Fluid Mech.* **198**, 365–386.

HENDERSON, L. F., COLELLA, P. & PUCKETT, E. G. 1991 On the refraction of shock waves at a slow-fast gas interface. *J. Fluid Mech.* **224**, 1–27.

HENSHAW, W. D., SMYTH, N. F. & SCHWENDEMAN, D. W. 1986 Numerical shock propagation using geometrical shock dynamics. *J. Fluid Mech.* **181**, 519–545.

JAHN, R. G. 1956 The refraction of shock waves at a gaseous interface. *J. Fluid Mech.* **1**, 457–489.

LINDL, D. L., MCCRORY, R. L. & CAMPBELL, E. M. 1992 Progress toward ignition and burn propagation in inertial confinement fusion. *Physics Today*, pp. 32–40, September.

MESHKOV, E. E. 1969 Instability of a shock wave accelerated interface between two gases. *Izv. Akad. Nauk. SSSR, Mekh. Zhidk. Gaza* **5**, 151. (*NASA Tech. Trans.* TT-F-13074, 1970.)

MULDER, W., OSHER, S. & SETHIAN, J. A. 1992 Computing interface motion in compressible gas dynamics. *J. Comput. Phys.*, **100**, 209–228.

PICONE, J. M. & BORIS, J. P. 1988 Vorticity generation by shock propagation through bubbles in a gas. *J. Fluid Mech.* **189**, 23–51.

PICONE, J. M. ORAN, E. S., BORIS, J. P. & YOUNG, T. R. 1983 Theory of vorticity generation by shock wave and flame interactions. *Presented at the 9th ICODERS, Poitiers, France, July 3-8.*

RICHTMYER, R. D. 1960 Taylor instability in shock acceleration of compressible fluids. *Commun. Pure Appl. Maths*, **XIII**, 297–319.

RUDINGER, G. & SOMMERS, L. M. 1960 Behaviour of small regions of different gases carried in accelerated gas flows. *J. Fluid Mech.* **7**, 161–176.

SAMTANEY, R. 1993 Vorticity in shock-accelerated density-stratified interfaces : An analytical and computational study. PhD Thesis, Rutgers University.

SAMTANEY, R. & ZABUSKY, N. J. 1992*a* Circulation and growth rate in Richtmyer-Meshkov instability using shock polar analysis. *Bull. Am. Phys. Soc.*, **37**, 1732.

SAMTANEY, R. & ZABUSKY, N. J. 1992*b* Visiometrics and reduced models for vorticity deposition in shock interactions with heavy cylindrical bubbles. *Caip Tech. Rep. 153, Rutgers University.*

SAMTANEY, R. & ZABUSKY, N. J. 1993 On shock polar analysis and analytical expressions for vorticity deposition in shock-accelerated density-stratified interfaces. *Phys. Fluids* A **5**, 1285–1287.

SCHWENDEMAN, D. W. 1988 Numerical shock propagation in non-uniform media. *J. Fluid Mech.* **188**, 383–410.

SILVER, D. & ZABUSKY, N. J. 1992 Quantifying visualizations for reduced modeling in nonlinear science: Extracting structures from data sets. *J. Visual Commun. Image Representation* **4**, 46–61.

SMOLLER, J. 1982 *Shock Waves and Reaction-Diffusion Equations.* Springer.

STRANG, G. 1968 On the construction and comparison of difference schemes. *SIAM J. Numer. Anal.* **5**, 506–517.

STURTEVANT, B. 1985 Rayleigh–Taylor instability in compressible fluids. *Caltech Report.* Unpublished.

VAN LEER, B. 1977 Towards the ultimate conservative scheme IV: A new approach to numerical convection. *J. Comput. Phys.* **23**, 276–299.

WINKLER, K.-H., CHALMERS, J. W., HODSON, S. W., WOODWARD, P. R & ZABUSKY, N. J. 1987 A numerical laboratory. *Physics Today* **40**(10), 28–37.

YANG, J., KUBOTA, T. & ZUKOSKI, E. E. 1993 Applications of shock-induced mixing to supersonic combustion. *AIAA J.* **31**, 854–862.

YANG, X., CHERN, I.-L., ZABUSKY, N. J., SAMTANEY, R. & HAWLEY, J. F. 1992 Vorticity generation and evolution in shock-accelerated density-stratified interfaces. *Phys. Fluids* A, **4**, 1531–1540.

ZABUSKY, N. J., SAMTANEY, R., YANG, X., CHERN, I.-L. & HAWLEY, J. F. 1992 Vorticity deposition, evolution and mixing for shocked density-stratified interfaces and bubbles. In *Shock Waves.*, (ed. K. Takayama). *Proc. 18th Intl. Symp. on Shock Waves, Sendai, Japan. Springer Verlag., July 21–26.* Springer.